Master thesis

Fractons in the U(1)-symmetry enriched Toric Code

Presented by

Maximilian Bernhard Johannes Vieweg

8.7.2024

Theoretische Physik
Friedrich-Alexander-Universität Erlangen-Nürnberg

Supervisors: Prof. Dr. Kai P. Schmidt, Andreas Schellenberger, Lea Lenke, Viktor Kott

Abstract

The $U(1)$-symmetry enriched toric code is investigated. It was shown before by using quantum Monte Carlo simulations that this model has a number of peculiar properties, like UV/IR mixing and Hilbert space fragmentation. In this thesis, a perturbative approach to the model was taken. By introducing an anisotropic star coupling, a new Hamiltonian called checkerboard $U(1)$-toric code is introduced that is exactly solvable in one limit and reproduces the $U(1)$-symmetry enriched toric code in another limit. Degenerate perturbation theory is used to study the model from the exactly solvable limit. Only diagonal corrections to the exactly solvable Hamiltonian are found and in fourth order perturbation theory, the ground state degeneracy is lifted and a global ground state is found. The excitations in this global ground state are investigated, and a non-topological phase of confined fractons is found. On finite systems, we investigate if the excitations found in the $U(1)$-symmetry enriched toric code still behave like fractons. The results are consistent with fractonic excitations.

Contents

I Introduction

The Landau theory of phase transitions is one of the most important cornerstones of modern condensed matter physics. In this theory, phase transitions are characterized by spontaneous symmetry breaking and a local order parameter that allows one to distinguish the different phases [1]. For a long time, this paradigm was applicable to all phase transitions. But the discovery of the fractional quantum Hall effect in 1982 changed this perception. The phase transitions to the fractional quantum hall states cannot be described by a local order parameter. Aside from this, the phases have many other exotic properties, like anyonic excitations that have a wave function that is neither symmetric nor anti symmetric under exchange of particles and a ground state degeneracy depending on the genus of the space the system is put on [2]. The system is in a so called topologically ordered phase [3]. The discovery of the fractional quantum Hall effect has sparked this new field of research, and both the experimental discovery by Daniel Tsui and Horst Störmer and the large progress in the theoretical description of this phase by Robert Laughlin were honored with the Noble Prize in 1998. The fractional quantum Hall effect is still an active research area, but the notion of topologically ordered phases has much further reaching impact.
The possibility of creating a system with non Abelian anyons, excitations where even the order of exchanging the particle is important, led the physicist Alexei Kitaev to the idea of building a quantum computer stable to local decoherence using the braiding properties of these exotic particles [4],[5]. It was also Kitaev who had the idea for a quantum stabilizer code, the toric code [5]. This model is topologically ordered and could be used for quantum error correction, but it is hard to realize in experiments since it has four-body interactions that are not found in nature. 20 years after its discovery, experiments have been performed to create the ground state of this model on quantum hardware [6], but an implementation of the model in a real physical system is still not possible. One possible way to create systems like the toric code is by using a symmetry principle called combinatorial gauge symmetry [7]. Here the fact is used that the commutation algebra of a spin system is not only invariant under $\bigotimes_i SU_i(2)$ transformations, but also under the exchange of different spins. In this way, a large class of Hamiltonians similar the toric code can be realized. An example of a model that can be realized in this way is the so-called WXY model [8]. The WXY model is hard to study numerically due to a sign problem and a large unit cell. In order to study the model, a simpler model with the same key properties, a global $U(1)$ symmetry, a

local $\mathbb{Z}_2$ symmetry and a similar structure, but without a sign problem was introduced. This model is the $U(1)$-symmetry enriched toric code [9]. In their work, Kai-Hsin Wu et. al. found evidence for a topologically ordered gapped quantum spin liquid with a lot of peculiar properties like UV/IR mixing and Hilbert space fragmentation. Theses findings are based on nummerical quantum Monte Carlo simulations, since the $U(1)$-symmetry enriched toric code is not exactly solvable as its conventional counter part.
In this thesis, the $U(1)$-symmetry enriched toric code is studied. First, a perturbative approach is taken to the model by going into a still exactly solvable limit. By using this approach, we find a non-topological phase with exotic excitations called fractons [10, 11]. These fractons are confined and cannot exist as single excitations but only as bound states. We discuss the possibility of a quantum phase transition to the topologically ordered phase. By using exact diagonalization, we study the properties of certain excitations in the $U(1)$ toric code phase and find results in line with the possibility of fractonic excitations in that phase as well.
This thesis is structured as follows: In chapter 2 the conventional toric code is introduced and the exact solution is presented. Than the different properties of the model are discussed, while focusing on the ones relevant for the $U(1)$-toric code. In chapter 3 the $U(1)$-toric code is introduced and the findings and discussion of Ref. [9] are summarised. In chapter 4 a new Hamiltonian is introduced that reproduces the $U(1)$-toric code for suited parameters but is still solvable in another limit. Starting from this still exactly solvable limiting case, perturbation theory is applied and a non topological phase with confined fractons is found. The possibility of a phase transition to a topological order phase is discussed. In chapter 5 heuristic arguments for the existence of fractons in the $U(1)$-toric code are presented and exact diagonalisation is used to check this reasoning.

II Toric Code

The toric code is an exactly solvable spin model introduced by Alexei Kitaev in Ref.[5]. The model is the simplest known model exhibiting topological order and has inspired tremendous research since it was discovered. In this chapter, we will introduce the model, show how it can be solved exactly, and then discuss some key properties, focusing on the ones that are relevant for the analysis of the $U(1)$-toric code.

II.1 Hamiltonian

The toric code was originally defined on a square lattice in two dimensions. We stick to this definition even though generalizations to different lattices [12, 13] and higher dimensions [14, 15] are possible. The spin degrees of freedom are placed on the links of the square lattice. Stars and plaquettes are defined as the spins closest to a vertex or on the site of a plaquette of the lattice, as seen in Figure II.1.

The Hamiltonian consists of star and plaquette operators (also called charges and fluxes). They are defined as

$$A_s = \prod_{i \in s} \sigma_i^x, \qquad B_p = \prod_{i \in p} \sigma_i^z, \tag{II.1}$$

where the product runs over the four indices of a star or a plaquette and $\sigma^{x/z}$ are the usual Pauli matrices.

The toric code Hamiltonian is then defined to be

$$H_{\mathrm{TC}} = -\sum_s A_s - \sum_p B_p, \tag{II.2}$$

with the sums running over all stars s and plaquettes p.

The important property that makes the model solvable are the vanishing commutators

$$[A_s, A_{s'}] = [B_p, B_{p'}] = [A_s, B_p] = 0 \quad \forall s, p, s', p'. \tag{II.3}$$

The first two commutators vanish trivially. The third one vanishes because plaquettes and stars share an even number of sites (see Figure II.2). Using this and $\sigma^z\sigma^x = -\sigma^x\sigma^z$ II.3 follows.

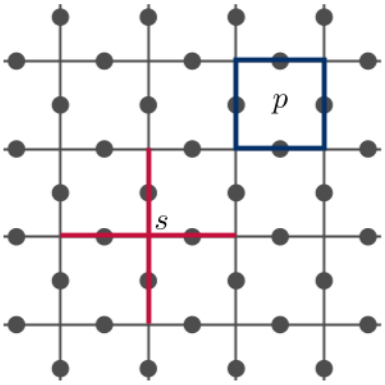

Figure II.1: Definition of stars and plaquettes on the square lattice

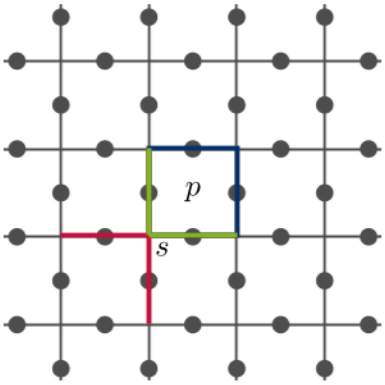

Figure II.2: Plaquettes and stars share two sites

Since the Hamiltonian is a sum of A_s and B_p, the commutator of the Hamiltonian with A_s and B_p gives

$$[H_{\mathrm{TC}}, A_s] = [H_{\mathrm{TC}}, B_p] = 0 \quad \forall s, p. \tag{II.4}$$

Because $(\sigma^i)^2 = \mathbb{1}$

$$A_s^2 = B_p^2 = \mathbb{1} \tag{II.5}$$

holds.

From Equation II.5, one can deduce that the eigenvalues of A_s and B_p, which we denote a_s and b_p respectively, can only be ± 1. With II.4, we see that there is a basis in which H_{TC}, A_s, and B_p are simultaneously diagonal. Choosing periodic boundary conditions we find that

$$\prod_s A_s = \prod_p B_p = \mathbb{1} \tag{II.6}$$

because on every spin, two star or plaquette operators act on.

Identity II.6 shows that not all a_s and b_p can be independent since fixing $N-1$ star eigenvalues a_s fixes the last a_s when N is the number of stars in the lattice. The analogous statement is true for b_p. So, A_s and B_p do not give a complete set of conserved quantities since the number of degrees of freedom N exceeds the number of eigenvalues. There are two more independent conserved quantities, with which A_s and B_p completely determine the eigenstate of the toric code. These are Wilson loop operators

$$W_\gamma^z = \prod_{i \in \gamma} \sigma_i^z \tag{II.7}$$

where γ is a non-contractible loop on the torus. On the torus, there are two topologically non-equivalent, non-contractible loops. Each of these gives an additional independent conserved quantity because W_γ^z can not be represented by a product of B_p operators (since γ is non-contractible) and

$$[H_{\mathrm{TC}}, W_\gamma^z] = 0. \tag{II.8}$$

One recognizes that this operator commutes trivially with all B_p, and every non-contractible loop shares an even number of sites with the A_s operators. Following the same argument as in the derivation of Equation II.3, we find Identity II.8.

II.2 Ground state manifold

To construct the ground state manifold of the toric code, all a_s and b_p have to be fixed to $+1$. One can construct a state that fulfills these constrains by starting with a reference state completely polarized in z direction $|\Uparrow\rangle$. Such a state clearly fulfills

$$B_p |\Uparrow\rangle = |\Uparrow\rangle . \tag{II.9}$$

To create a state with $a_s = +1$ for all stars, one can use that $\frac{\mathbb{1}+A_s}{2}$ is a projector to the eigenspace with eigenvalue $a_s = +1$. That $\frac{\mathbb{1}+A_s}{2}$ is a projector to the eigenspace $a_s = +1$ is easily checked by calculating $(\frac{\mathbb{1}+A_s}{2})^2 = \frac{\mathbb{1}+A_s}{2}$ and $A_s \frac{\mathbb{1}+A_s}{2} = \frac{\mathbb{1}+A_s}{2}$ using Equation II.5. Hence,

$$\mathcal{N} \prod_s \frac{\mathbb{1} + A_s}{2} |\Uparrow\rangle = |\mathrm{gs}\rangle \tag{II.10}$$

gives a ground state with $a_s = +1$ and $b_p = +1$ for all stars and plaquettes with a normalization constant $\mathcal{N}$.
Calculating the product in Equation II.10 gives

$$\mathcal{N}(\mathbb{1} + \sum_s A_s + \sum_{s'<s} A_s A_{s'}) + ...) |\Uparrow\rangle = |\mathrm{gs}\rangle \tag{II.11}$$

which is an equal-weight superposition of all states of the form $\prod_{s\in\mathcal{M}} A_s |\Uparrow\rangle$ where $\mathcal{M}$ is a subset of stars on the lattice. The action of σ^x on a σ^z product state is a spin flip, i.e. $\sigma^x |\uparrow\rangle = |\downarrow\rangle$. A_s acting on a $|\Uparrow\rangle$ flips all spins on the star s. The flipped spins form a contractible loop on the torus, as it can be seen in Figure II.3. The ground state is then an equal weight superposition of all those contractible loop states.

Because $[\frac{\mathbb{1}+A_s}{2}, W_{1/2}^z]$ vanishes $W_{1/2}^z |\mathrm{gs}\rangle = + |\mathrm{gs}\rangle$ holds. To construct the other ground states, an operator $W_\alpha^x = \prod_{i\in\alpha} \sigma_i^x$ where α is a non-contractible loop around the torus on the dual lattice can be defined. $W_\alpha^x = \prod_{i\in\alpha} \sigma_i^x$ commutes with the B_p and A_s

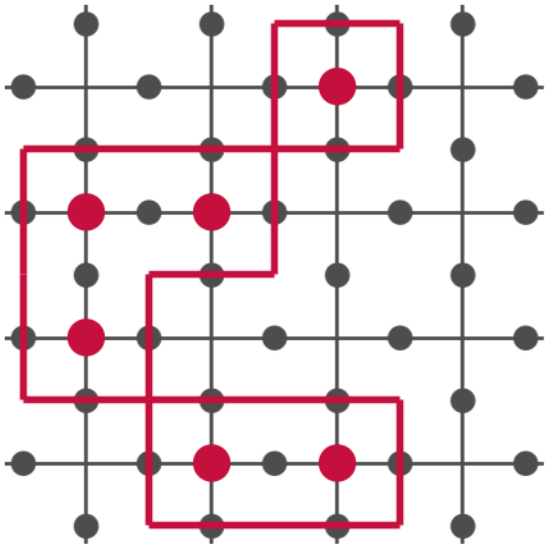

Figure II.3: An example for a loop state in σ^z basis. The red dots show all the stars s A_s acted on, and the red lines visualize the loop of flipped spins

.

for all s and p but changes the eigenvalue of one of the Wilson loops $W^z_{1/2}$. By this construction, one can obtain all four ground states: $|\text{gs}, 1, 1\rangle$, $|\text{gs}, -1, 1\rangle$,$|\text{gs}, 1, -1\rangle$ and $|\text{gs}, -1, -1\rangle$ where the last two arguments give the eigenvalues of $W^z_{1/2}$. This way, one sees that the ground state degeneracy is 4^g where g is the number of non-contractible loops on the manifold (the genus of the manifold). This is an important property of topological ordered phases.

II.3 Mutual anyonic statistics

The spin statistics theorem states that spin $\frac{1}{2}$ particles have an anti-symmetric wave function under particle exchange, and spin one particles have a symmetric wave function under particle exchange. Further, in three or more spatial dimensions, it also states that the wave function has to be symmetric or anti symmetric. In two spatial dimension there is a loophole in the theorem, which results in a much richer theory and leads to fascinating new excitations called anyons. Abelian anyons get a phase factor when exchanged. In this section, we derive the symmetry of the toric code exitations and find that the excitations are indeed Abelian anyons [4].

We can only have an excitation in the toric code if one of the constraints $b_p = 1$ or $a_s = 1$ is violated. With condition II.6, we find that creating only one excitation is impossible on the torus. Creating two excitations can be done by acting with the string operators $S^z(t) = \prod_{i\in t} \sigma^z$, $S^x(t') = \prod_{i\in t'} \sigma^x$. t is a path on the lattice and the excitations are induced on the stars t' is a path on the dual lattice and the excitations are on the plaquettes. In Figure II.4 an example for the creation of two excitations is shown. Acting with $S^z(t)$ on the ground state gives

$$S^z(t)\,|\mathrm{gs}\rangle = S^z(t)\prod_s \frac{\mathbb{1}+A_s}{2}\,|\Uparrow\rangle = \frac{\mathbb{1}-A_{s_1}}{2}\frac{\mathbb{1}-A_{s_2}}{2}\prod_{s\neq s_1,s_2}\frac{\mathbb{1}+A_s}{2}S^z(t)\,|\Uparrow\rangle \tag{II.12}$$

where s_1 and s_2 are the stars on which the loop t ends and the only stars that share only one spin with the open string t. $\frac{\mathbb{1}-A_s}{2}$ is a projector on the eigenvalue -1 for the star s. With the analog argument, one sees that $S^x(t')\,|\mathrm{gs}\rangle$ is the state with two plaquettes excitations at the end of string t'. With this construction, W^x can be interpreted in this particle picture as creating two excitations and moving them around a non-contractible loop before annihilating them again.
We discuss the statistics of the particles now. The star excitations behave as bosons when they are exchanged with another star excitation. This is also true for the plaquette excitations. The mutual exchange statistic is more interesting.
To discuss the mutual Abelian statistic, we look at an excited state $S^z(t)S^x(t')\,|\mathrm{gs}\rangle$ with both types of excitation (for example, the state in figure II.4). Now the star excitation can be moved around the plaquette excitation by acting with $S^z(\gamma)$. The loop γ winds around the plaquette excitation like illustrated in II.5. Since t' and γ have to share an uneven number of sites, we find

$$S^z(\gamma)S^z(t)S^x(t')\,|\mathrm{gs}\rangle = -S^z(t)S^x(t')S^z(\gamma)\,|\mathrm{gs}\rangle = -S^z(t)S^x(t')\,|\mathrm{gs}\rangle\,, \tag{II.13}$$

where we used in the last step that every contractible loop can be represented by a product of B_p operators and $B_p\,|\mathrm{gs}\rangle = |\mathrm{gs}\rangle$. Moving the particles around each other is equivalent to exchanging them twice. With this argument, we find that exchanging the particles once gives a factor of $e^{i\pi/2}$. So we find Abelian anyonic statistics.

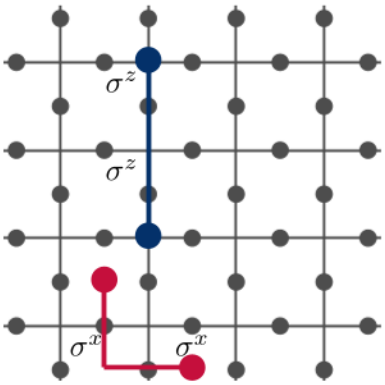

Figure II.4: Creation of anyons using $\sigma^{x/z}$.

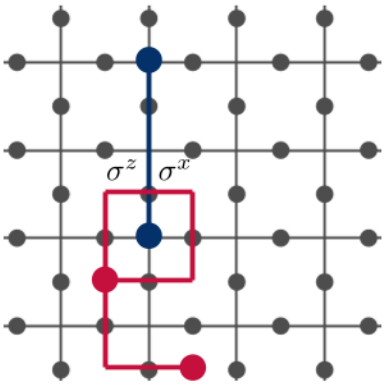

Figure II.5: Exchange of anyons.

III $U(1)$ symmetry enriched toric code

The $U(1)$ symmetry enriched toric code (also called $U(1)$ toric code) is a new model introduced by Kai-Hsin Wu et al. in [9]. In this chapter, we follow their work and show how to derive the Hamiltonian from the usual toric code. Then we give a summary of their numerical findings and a discussion of those.

III.1 Enriching the toric code by a $U(1)$ symmetry

The model can be introduced by altering the usual star operator

$$A_s = \sigma_1^x \sigma_2^x \sigma_3^x \sigma_4^x \tag{III.1}$$

so it is invariant under $U(1)$ symmetry transformations. One introduces a new angle-dependent Pauli matrix $\sigma^\theta = \cos(\theta)\sigma^x + \sin(\theta)\sigma^y$ and a new star operator

$$A_s^\theta = \prod_{i \in s} \sigma_i^\theta, \tag{III.2}$$

where the sites lie on the star like in the usual toric code. These operators still commute with the B_p operators and each other. The new $U(1)$ symmetry is now introduced by integrating over all angles

$$\tilde{A}_s = \int_0^{2\pi} A_s^\theta \mathrm{d}\theta = \sigma_1^+ \sigma_2^+ \sigma_3^- \sigma_4^- + \sigma_1^+ \sigma_2^- \sigma_3^+ \sigma_4^- + \sigma_1^+ \sigma_2^- \sigma_3^- \sigma_4^+ + \textbf{h.c.} \tag{III.3}$$

with $\sigma^\pm = \frac{(\sigma^x \pm i\sigma^y)}{2}$. The Hamiltonian is then given by

$$H_{U(1)} = -\lambda_A \sum_s \tilde{A}_s - \lambda_B \sum_p B_p \tag{III.4}$$

where $\lambda_{A/B} > 0$. First, we notice $[B_p, \tilde{A}_s] = 0$ still holds true for all s and p, but $[\tilde{A}_s, \tilde{A}_s'] \neq 0$ if s and s' share a site. This makes it impossible to solve the system in any obvious analytical way. We now check how the $U(1)$ symmetry enters the system. We introduce the action of the $U(1)$ symmetry group

$$U_z = \exp\left(-i\frac{\alpha}{2} M_z\right) \tag{III.5}$$

with the total magnetization in z-direction $M_z = \sum_i \sigma_i^z$. The action of the symmetry on σ^θ is

$$U_z \sigma^\theta U_z^\dagger = \sigma^{\theta+\alpha}, \tag{III.6}$$

so we obtain

$$U_z \tilde{A}_s U_z^\dagger = \int_0^{2\pi} U_z A_s^\theta U_z^\dagger d\theta = \int_0^{2\pi} A_s^{\theta+\alpha} d\theta = \tilde{A}_s. \tag{III.7}$$

The action of U_z on B_p is trivial, so we obtain that $H_{U(1)}$ is invariant under these transformations. Like every symmetry, this symmetry has an associated conserved quantity. Here, this quantity is the total magnetisation M_z. As we have seen above, all the B_p still commute with the Hamitonian, so the eigenvalues b_p are also conserved. In addition, the Wilson loops defined for the toric code fulfill $[H_{U(1)}, W_\gamma^z] = 0$ so they give conserved quantities as well. With all these conserved quantities, we can block-diagonalize the system with blocks labeled by the eigenvalues of the operators $\{M_z, W_1, W_2, \{B_p\}\}$.

Another property of the Hamiltonian is that it exhibits Hilbert space fragmentation. This property was described first in Refs. [16, 17]. For systems with this property, the Hamiltonian has a block diagonal structure even inside each symmetry sector. The blocks are so called Krylov sectors. These Krylov sectors are not explained by any (obvious) symmetry since the operators with whom one would explain them are highly nontrivial and nonlocal projectors on those blocks, which cannot be constructed easily. Systems exhibiting this property are known to violate the eigenstate thermalization hypothesis (ETH) [18]. The ETH is a condition most Hamiltonians obey under which equilibrium statistical mechanics is recovered from quantum systems in isolation. Other examples of systems that violate ETH are those with quantum scars or many body localisation [18]. There are two types of Hilbert space fragmentation: strong and weak fragmentation [19]. For strong fragmentation, $D_{\max}/D_{\text{complete}} \longrightarrow 0$ for $L \longrightarrow \infty$ while for weak fragmentation, $D_{\max}/D_{\text{complete}} \longrightarrow 1$ for $L \longrightarrow \infty$. $D_{\max}$ is the dimension of the largest Krylov subspace in the symmetry sector, while D_{complete} is the dimension of the whole symmetry sector, and L is the system size. The dynamics of the symmetry sector $(+,+)$ can be mapped to a model that is known to exhibit weak Hilbert space fragmentation [20, 21, 22]. For the other subsectors, this was established numerically in Ref [9]. In Figure III.3 an example of how this fragmentation manifests can be seen.

III.2 Previous numerical findings

In this section, some of the numerical findings by Kai-Hsin Wu et al. [9] are summarized. They used exact diagonalization (ED) and Stochastic Series Expansion Quantum Monte Carlo (SSE QMC) for their numerical study. They choose $\lambda_A \ll \lambda_B$ so that

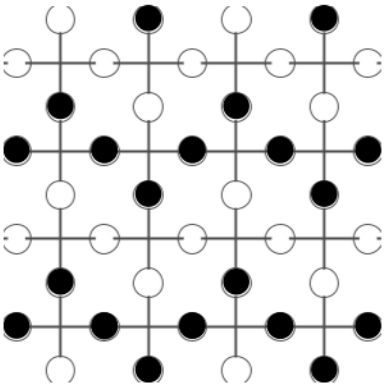

Figure III.1: Example of a completely frozen product state. Black dots denote $|\uparrow\rangle$, while white dots are $|\downarrow\rangle$ states. $\tilde{A}_s$ projects the state to zero, independent of the star it acts on.

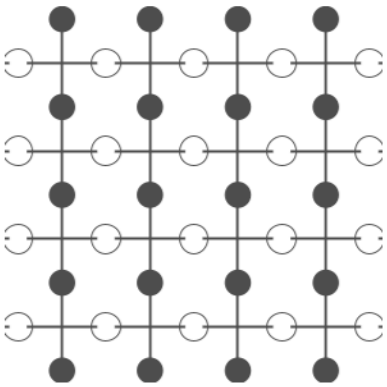

Figure III.2: $\tilde{A}_s$ can act on every star without projecting the state to 0.

Figure III.3: Example of states corresponding to the same symmetry sector but different Krylov subspaces. The left state belongs to a one dimensional subspace, while the left state belongs to a higher dimensional one. Rebuild version of Figure 7 from [9]

the global ground state is in the symmetry sector where all B_p eigenvalues are $+1$. The eigenvalue of M_z was chosen to be $m_z = 0$. This is the symmetry sector in which the global ground state is expected. This is easy to see since this symmetry sector has the highest dimension and the spread of eigenvalues is larger for larger random matrices. This was verified for small systems. They used ED to verify the Hilbert space fragmentation in all symmetry sectors and benchmark their QMC study. When fixing all these quantities, the Wilson loops still remain. The symmetry sectors are labeled by the sign of the corresponding eigenvalues of $W_{1/2}$ $(+,+),(+,-),(-,+)$, and $(-,-)$, where the first entry is the sign of W_1 and the second of W_2. They studied different compactifications. A compactification is a way of defining the periodic boundary condition. The compactifications they studied all have the topology of a torus, so for the usual toric code, one would see that the ground state degeneracy does not depend on the compactification. For the $U(1)$ toric code, a different behavior was found.

The different discussed compactifications are characterized by two coprime integers a, b and the linear system size L. This then gives two compactification vectors: $\vec{L}_1 = (-b\vec{e}_x + a\vec{e}_y)$ and $\vec{L}_2 = (a\vec{e}_x + b\vec{e}_y)$. Any vector $\vec{r}$ is identified with all $\vec{r} + m\vec{L}_1 + n\vec{L}_2$ for $n, m \in \mathbb{Z}$. The vectors (a, b) and $(-b, a)$ are the shortest vectors with integer

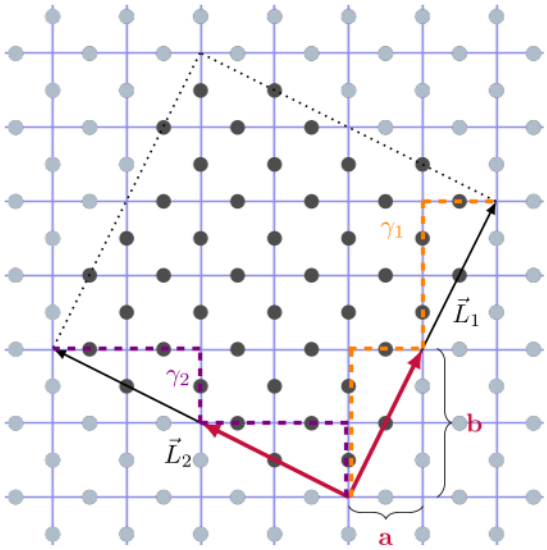

Figure III.4: An example for a compactification with $a = 1$, $b = 2$, and system size $L = 2$. The black vectors are the compactification vectors $\vec{L}_1$ and $\vec{L}_2$ and are identified with the black dotted lines on the opposing side of the square. The yellow and violet dotted lines are two independent non-contractible loops γ_1 and $/\gamma_2$. The picture is a rebuilt version of figure 1 in [9].

.

coefficients in the direction of the compactification vectors. An example of such a compactification can be seen in III.4. In their work, Kai-Hsin Wu et al. focused especially on compactifications characterized by even linear system size L and the two vectors $(a = 1, b = 1)$ and $(a = 1, b = 0)$. These compactifications are called 0° and 45° compactification and are also the most relevant ones for this thesis.
The first and most important finding is the dependence of the ground state degeneracy on the compactification. For the 0° compactification, the global ground states lie in the symmetry sectors $(+,+)$ and $(-,-)$ for large and even L. These two ground states are degenerated. The lowest energy states in the sectors $(+,-)$ and $(-,+)$ have a higher energy with a gap of $O(1)$ in system size L. In the 45° compactification, the global ground states for large and even L lie in the symmetry sectors $(+,+)$,$(-,+)$, and $(+,-)$. The ground state in the symmetry sector $(-,-)$ is an excited state again with a gap of $O(1)$ in system size L. To check if the system is gapped within each symmetry sector, spin-spin correlations were calculated. Particularly, the expectation value of the operators $C(r) = \frac{1}{L}\sum_\alpha \sigma^z_{\vec{e}_x+\alpha\vec{e}_y}\sigma^z_{\vec{e}_x+\alpha\vec{e}_y+r\vec{x}}$ and $C_d(r) = \frac{1}{L}\sum_\alpha \sigma^z_{\vec{e}_x+\alpha\vec{e}_{\tilde{x}y}}\sigma^z_{\vec{e}_x+\alpha\vec{e}_{\tilde{x}y}+r\vec{e}_{xy}}$. The correlations decay to zero for $r \geq 3$ which is seen as strong evidence that the system is gapped within each symmetry sector. Furthermore, the star-star correlation

function $\langle \tilde{A}_s \tilde{A}_{s'} \rangle$ was calculated. By fixing $s = (0, 0)$ and plotting the correlation function for $s' = (x, y)$ a checkerboard pattern was found like seen in Figure III.5. This indicates a breaking of translation symmetry, and due to this, there is an additional two fold degeneracy within each symmetry sector. This additional degeneracy is not topological and can be lifted by local perturbations.

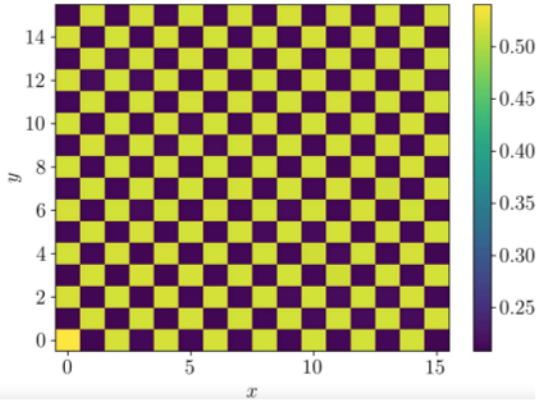

Figure III.5: Plot of the correlation function $\langle \tilde{A}_s \tilde{A}_{s'} \rangle$ for linear system size $L = 16$ further motivating the approach later mentioned in the thesis. The plot is taken from Ref. [9].

.

III.3 Ground state degeneracy

In this section, we follow the discussion of Chapter 4 in Ref. [9] on the ground state degeneracy and their heuristic argument to explain it. Later in the thesis, this argument are put in the context of fractonic excitations.
The numerical results for the ground state degeneracy are interesting for two reasons: The first one is the dependency of the ground state degeneracy on the compactification. The compactification is a detail of the lattice. The ground state degeneracy on the other hand is a property predicted by the low energy effective field theory (a topological quantum field theory for ususal topolgical order) that describes the phase (like the doubled Chern-Simons theory also called BF theory [23] for the usual toric code). So a detail of the lattice, which is relevant for short wavelengths (or equivalently high energies), influences the low energy effective field theory, which determines the physics at long wavelengths (or low energies). This phenomenon is known as UV/IR mixing [24, 25]. UV/IR mixing is common for gapped fracton phases, but in those systems the ground state degeneracy usually depends on the system size [10, 11]. A dependence on the compactification is unusual.

The second reason why the ground state degeneracy is interesting is the three fold topological ground state degeneracy in the 45° compactification. It is unusual to get such a degeneracy from a time reversal symmetric Hamiltonian with Abelian topological order. Topological quantum field theories usually have a ground state degeneracy, which is either the square of an integer or a product of Pythagorean primes (for time reversal symmetric $U(1)_k$ Chern-Simons theories this was proven in ref.[26]). 3 is neither a square of an integer nor a Phythagorean prime. An explanation would be that the time reversal symmetry is broken spontaneously.

Long range magnetic order provided no evidence for this possibility since the ground state lie in the symmetry sector with $M_z = 0$ and the spin-spin correlation functions decay exponentially.
Motivated by this question, Kai-Hsin Wu et. al. took a phenomenological approach to explain the ground state degeneracy. They proposed the existence of nonlocal tunneling operators T_1 and T_2, which change the eigenvalues of the Wilson loop operators W_1 and W_2. For the toric code, the analog construction would be the W^x_γ operator. For the $U(1)$ toric code, these operators cannot be constructed explicitly. Considering the 45° compactification we call these operators $T_1^{45^\circ}$ and $T_2^{45^\circ}$. The three ground states are then given by $|(+,+)\rangle$, $T_1^{45^\circ}|(+,+)\rangle = |(-,+)\rangle$ and $T_2^{45^\circ}|(+,+)\rangle = |(+,-)\rangle$. The last state $|(-,-)\rangle$ was found to be an excited state. So $T_2^{45^\circ}T_1^{45^\circ}|(+,+)\rangle$ is orthogonal to the ground state manifold or, equivalently, $T_2^{45^\circ}T_1^{45^\circ}$ annihilates $|(+,+)\rangle$ on the ground state manifold.
The same situation is found in $SU(2)_2$ topological order with Ising anyons as excitations where one cannot insert anyons along both noncontractible loops without projecting to 0 [27]. This observation led the authors of [9] to the conclusion that the 45° compactification could host non abilian anyons.
Based on this phenomenological argument they proposed a heuristic argument to explain the ground state degeneracy in the 0° compactification. Acting with $T_i^{45^\circ}$ in the 0° compactification the operator winds around ±45° direction. In this direction the operator changes both eigenvalues of the Wilson loop operators so we obtain $T_i^{45^\circ}|(+,+)\rangle = |(-,-)\rangle$. The states $|(+,-)\rangle$ and $|(-,+)\rangle$ are not accessible in this way.

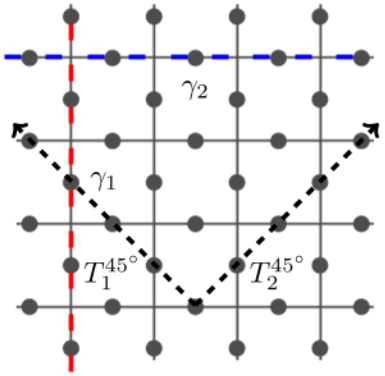

Figure III.6: The tunneling operators act diagonally and change both eigenvalues of W_1^z and W_2^z.

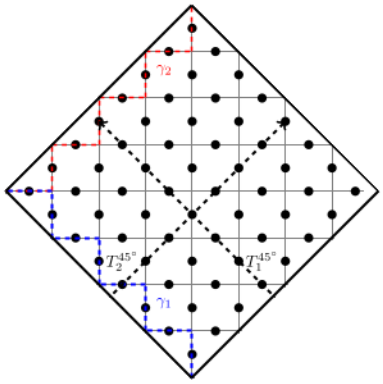

Figure III.7: The tunneling operators for the 45° compactification. The operator crosses only one noncontractible loop, W_1^z or W_2^z and changes its eigenvalue.

IV Perturbation theory applied to the checkerboard $U(1)$ toric code

In this chapter, the perturbative approach introduced by Minoru Takahashi in Ref. [28] is applied to study the $U(1)$ toric code by introducing an anisotropic star coupling. After choosing a suitable yet exactly solvable unperturbed Hamiltonian and calculating the effective Hamiltonian up to fourth order, a confined fracton phase without topological order is found.

IV.1 Unperturbed Hamiltonian and ground state $0°$ tilt

To use perturbation theory, a simple, exactly solvable unperturbed Hamiltonian is needed. As seen in Chapter 3, the Hamiltonian for the $U(1)$ toric code can not be solved exactly due to the non-vanishing commutators $[\tilde{A}_{s_1}, \tilde{A}_{s_2}]$ when s_1 and s_2 are neighbors. But if s_1 and s_2 have no common site, $[\tilde{A}_{s_1}, \tilde{A}_{s_2}] = 0$ still holds. Motivated by this, the stars can be separated into two bipartite sublattices, S' and S'', where every second star is in sublattice S', and two new parameters are introduced, so the strength of the stars on the sublattices differs. The new Hamiltonian reads

$$H_{U(1),\mathrm{CB}} = -\lambda_B \sum_p B_p - \lambda_{A'} \sum_{s' \in S'} \tilde{A}_{s'} - \lambda_{A''} \sum_{s'' \in S''} \tilde{A}_{s''}, \tag{IV.1}$$

with new couplings $\lambda_{A'}, \lambda_{A''} > 0$. This Hamiltonian we refer to as the checkerboard $U(1)$ toric code, and it reproduces the Hamiltonian of the $U(1)$ toric code for $\lambda_{A'} = \lambda_{A''}$. The A_s on each sublattice commutes, so the Hamiltonian IV.1 is exactly solvable for $\lambda_{A''} = 0$.
Six of the local eigenstates of $\tilde{A}_s$ are given by

$$|w\rangle = \frac{1}{\sqrt{2}}(|1\rangle + |\bar{1}\rangle), \tag{IV.2}$$

$$|\tilde{w}\rangle = \frac{1}{\sqrt{2}}(|-1\rangle + |-\bar{1}\rangle), \tag{IV.3}$$

$$|v\rangle = \frac{1}{\sqrt{2}}(|0\rangle + |\bar{0}\rangle)) \tag{IV.4}$$

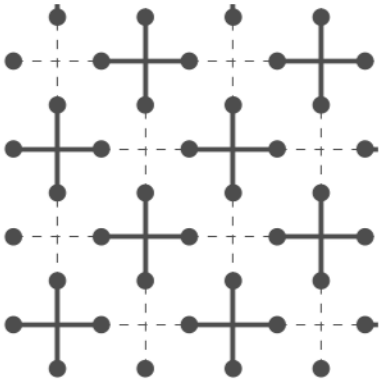

Figure IV.1: Separation in the sub lattices S' and S''. The thick stars are unperturbed and the dashed stars are the ones the perturbations act on.
.

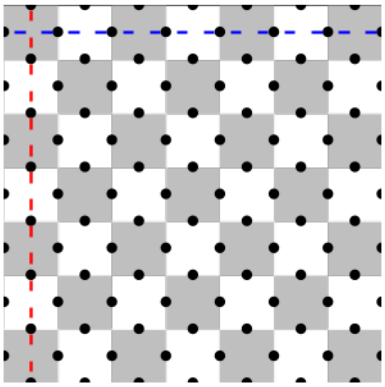

Figure IV.2: Different visualization of Figure IV.1. The gray squares correspond to unperturbed stars, and the white squares are the ones the perturbation acts on. The red and blue dashed lines are the non contractible loops the Wilson loop operator acts on.

and

$$|w_-\rangle = \frac{1}{\sqrt{2}}(|1\rangle - |\bar{1}\rangle), \tag{IV.5}$$

$$|\tilde{w}_-\rangle = \frac{1}{\sqrt{2}}(|-1\rangle - |-\bar{1}\rangle), \tag{IV.6}$$

$$|v_-\rangle = \frac{1}{\sqrt{2}}(|0\rangle - |\bar{0}\rangle)), \tag{IV.7}$$

where the states are defined like seen in Figure IV.3 and the corresponding eigenvalues are $+1$ if the sign in front of the second vector is $+1$ and -1 if it is -1. The remaining eigenvectors have the eigenvalue 0. They are given by product states that are not flippable and can be seen in Figure IV.5.

This ansatz explicitly breaks the translational symmetry, which is spontaneously broken in the full system. For $\lambda_B = 0$, all local ground states can independently be put on the checkerboard. So one finds for each unperturbed star three local ground states: $|v\rangle$, $|\tilde{w}\rangle$ and $|w\rangle$. We would expect a $3^{N_{\text{up}}}$ fold ground state degeneracy, where N_{up} is the number of unperturbed stars. Choosing $\lambda_B \neq 0$ new constraints are imposed on the ground states, and the ground state degeneracy changes. For a state to be part of the ground state manifold, all B_p eigenvalues need to be $+1$.

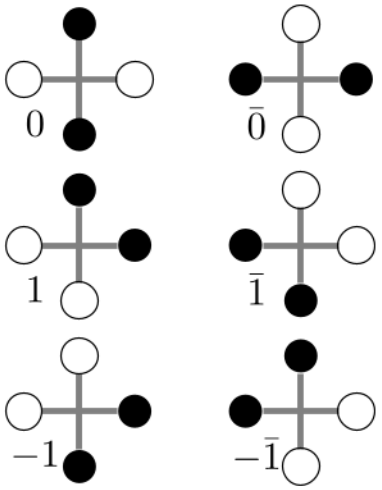

Figure IV.3: Labeling of all flippable product states.

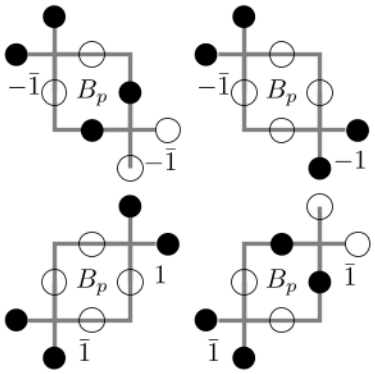

Figure IV.4: Constraints imposed by the plaquette eigenvalue +1.

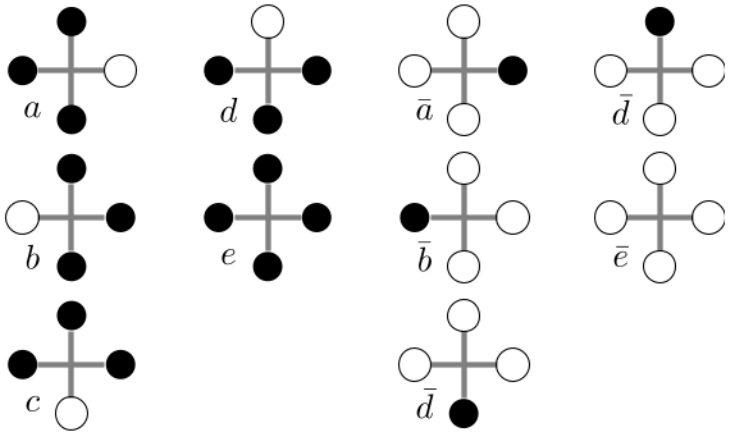

Figure IV.5: Local product states corresponding to the eigenvalue 0. These states are called non flippable states.

.

The local ground states are sums of the local product states defined in figure IV.3. These states are called flippable since they are the only local product states that are not projected to 0 if $\tilde{A}_s$ acts on them. The local product states give constraints on the neighboring product states of the checkerboard, if $B_p |\text{gs}\rangle = |\text{gs}\rangle$ is required.

$|1\rangle$ or $|\bar{1}\rangle$ share either 2 up or 2 down spins with the plaquette on the top right. So the state of the star on the top right also has to share 2 up or down spins with the plaquette for B_p to be 1. The only flippable states that fulfill this condition are $|1\rangle$ and $|\bar{1}\rangle$. The argument for $|-1\rangle$ and $|\bar{1}\rangle$ is analogous. With this, we can deduce the constraints a product state built out of flippable stars on the checkerboard has to fulfill so that $B_p |\Psi\rangle = |\Psi\rangle$. If the star on the bottom left of the plaquette is in the state $|1\rangle$ or $|\bar{1}\rangle$, the state on the top right has to be either $|1\rangle$ or $|\bar{1}\rangle$. If the state on the top left is $|-1\rangle$ or $|-\bar{1}\rangle$, the state on the bottom right has to be $|-1\rangle$ or $|\bar{-1}\rangle$.
Applying this constraint inductively, we find that one $|-1\rangle$ or $|\bar{-1}\rangle$ requires the whole diagonal to be $|-1\rangle$ or $|\bar{-1}\rangle$. And one $|1\rangle$ or $|\bar{1}\rangle$ requires the whole anti-diagonal to be $|1\rangle$ or $|\bar{1}\rangle$. The term anti-diagonal is used in the same way as for matrices.
Applying these constraints to the ground state manifold of the unperturbed Hamiltonian, we find that one $|w\rangle$ constrains the whole anti-diagonal to be in the state $|w\rangle$ and $|\tilde{w}\rangle$ the whole diagonal to be in the state $|\tilde{w}\rangle$.
We also notice that if we restrict all states on an anti-diagonal to be $|w\rangle$, there cannot be a diagonal with $|\tilde{w}\rangle$ since the diagonals would meet, and either the constrain given by the B_p has to be violated or a local eigenstate of the stars does not give the eigenvalue $+1$. With these arguments, we find a smaller ground state degeneracy than in the case where $\lambda_B = 0$. We can label the states in the unperturbed ground state manifold by the states on their diagonals or anti-diagonal. For a system of the size $L \times L$, the number of ground states is $2^{L+1} - 1$ in the 45° compactification and $2^{\frac{L}{2}+1} - 1$ in the 0° compactification with even L. The number of states where one or no diagonal is restricted to $|w\rangle$ is 2^{L_d} where L_d is the number of unperturbed (anti-) diagonals in the system. This is easy to see since L_d is equal to the number of diagonals, and with the restriction that no diagonal can be in the state $|\tilde{w}\rangle$, every diagonal can be restricted to be either $|w\rangle$ or $|v\rangle$. We get the same number of states if the anti-diagonal is restricted to be $|\tilde{w}\rangle$. But we double count the state where all local states are $|v\rangle$. For the 0° compactification and even system size $L_d = \frac{L}{2}$ and for the 45° compactification it equals L. It follows that the ground state degeneracy grows subextensive compared to the extensive ground state degeneracy in the case where $\lambda_B = 0$.
The eigenvalue of $W_{1/2}$ still has to be discussed. Acting with $W_{1/2}$ on a product state in σ^z basis gives $(-1)^{N_{up}}$ where N_{up} is the number of spins pointing up on the non-contractible loop. Here the non-contractible loops are defined like in figure IV.2.

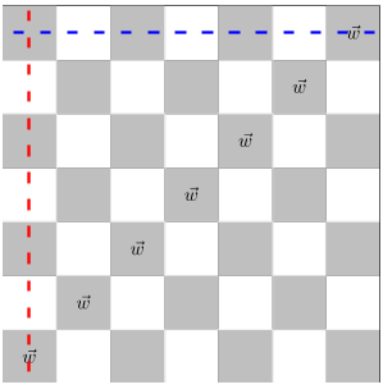

Figure IV.6: The picture shows an anti-diagonal constraint to be $|w\rangle$.

.

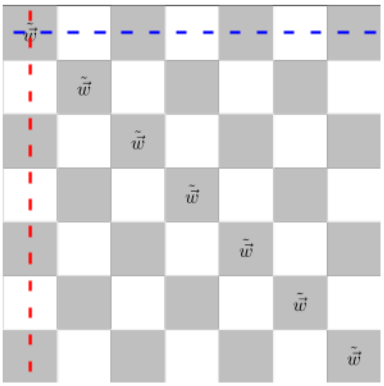

Figure IV.7: The picture show a diagonal constraint to be $|\tilde{w}\rangle$.

One can see, that the states $|0\rangle$ and $|\bar{0}\rangle$ contribute a factor of 1 to the eigenvalue of $W_{1/2}$ since the non-contractible loops cross the stars vertically or horizontally. As seen in Figure IV.3 the contribution to the product is either $(-1)^2$ or $(-1)^0$.

Analogously, all the other flippable stars contribute a factor (-1) to the product.

To determine the eigenvalue of a ground state, we calculate

$$W_{1/2}\,|w_s\rangle \otimes |\phi\rangle = \frac{1_s}{\sqrt{2}}\sigma_i^z\sigma_j^z(|1_s\rangle + |\bar{1_s}\rangle) \otimes \tilde{W}_{1/2}\,|\phi\rangle = -\,|w_s\rangle \otimes \tilde{W}_{1/2}\,|\phi\rangle \tag{IV.8}$$

$$W_{1/2}\,|\tilde{w}_s\rangle \otimes |\phi\rangle = \frac{1}{\sqrt{2}}\sigma_i^z\sigma_j^z(|-1\rangle + |-\bar{1}_s\rangle) \otimes \tilde{W}_{1/2}\,|\phi\rangle = -\,|\tilde{w}\rangle \otimes \tilde{W}_{1/2}\,|\phi\rangle \tag{IV.9}$$

$$W_{1/2}\,|v_s\rangle \otimes |\phi\rangle = \frac{1}{\sqrt{2}}\sigma_i^z\sigma_j^z(|0_s\rangle + |\bar{0}_s\rangle) \otimes \tilde{W}_{1/2}\,|\phi\rangle = |v\rangle \otimes \tilde{W}_{1/2}\,|\phi\rangle \tag{IV.10}$$

where $\tilde{W}_{1/2}$ is the Wilson loop operator acting on the remaining factor of the tensor product $|\phi\rangle$ and i and j are the indices on which the non-contractible loop crosses the star s the local star operator acts on. So the eigenvalue for a ground state built by local eigenstates is an eigenstate of both $W_{1/2}$. The eigenvalue is given by the number of local $|w\rangle$ and $|\tilde{w}\rangle$ states of the non-contractible loops as $(-1)^{N_{w,\tilde{w}}}$ where $N_{w,\tilde{w}}$ is the number of $|w\rangle$ and $|\tilde{w}\rangle$ states on the non contractible loop.

Since an (anti-)diagonal always crosses both non-contractible loops, every state on the checkerboard has the same eigenvalue for W_1 and W_2. Therefore, all ground states lay in the symmetry sectors $(+,+)$ and $(-,-)$. The global ground states of the system at $\lambda_A'' = 1$ are in the same symmetry sectors for the 0° compactification.

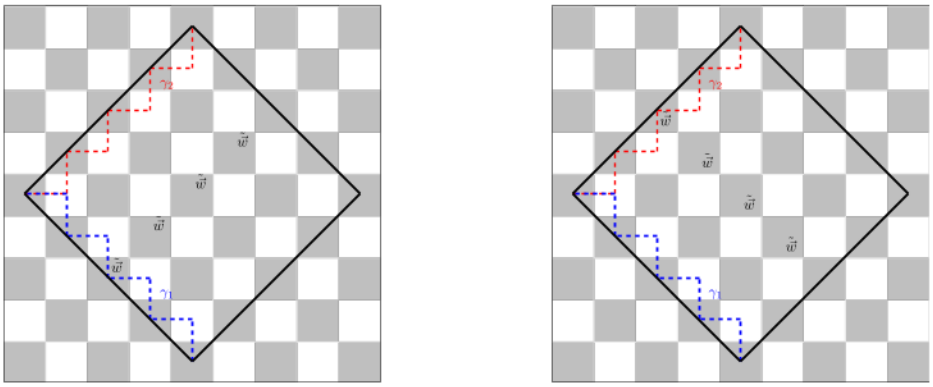

.

Figure IV.8: Constraints on the diagonal in the 45° compactification.

IV.2 Ground state for $45°$ compactification

The local eigenstates stay the same for other compactifications. Also, the arguments for the constraints do not change. But the states are now constrained parallel to the compactification vectors, as can be seen in Figure IV.8. This has interesting consequences for the symmetry sectors that the ground states lie in. First, we notice, analog to the section before, that the flippable local product states $|0\rangle$, $|\tilde{0}\rangle$, $|1\rangle$ and $|\bar{1}\rangle$ give a factor of -1 to the eigenvalue $w_2 = (-1)^{N_{\mathrm{up},1}}$ where $N_{\mathrm{up},1}$ is the number of spin-ups on the non-contractable loop γ_2 while $|1\rangle$ or $|\bar{1}\rangle$ give a factor $(+1)$. The reason is that the non-contractible loop always intersects the stars at the top and left. For the W_1 along the non-contractible loop γ_1 we find that the states $|0\rangle$, $|\tilde{0}\rangle$,$|-1\rangle$ and $|\bar{-1}\rangle$ give a factor -1 and the states $|-1\rangle$ or $|\bar{-1}\rangle$ a factor $+1$ with the analog argument.
Following the same argumentation as for the 0 degree compactification, we find that $|v\rangle$ and $|\tilde{w}\rangle$ give a factor -1 to the product w_1 and $|w\rangle$ gives a factor $+1$ to the product. For the product w_2 $|v\rangle$ and $|w\rangle$ give a factor of $+1$ and $|\tilde{w}\rangle$ gives a factor of -1.

With the constraints in mind and how the diagonals affect the eigenvalues of the Wilsone loop operators, we find that all ground states are in the symmetry sectors $(+,+)$, $(-,+)$, and $(+,-)$ for even L. We know that there can not be $|w\rangle$ and $|\tilde{w}\rangle$ states in a ground state built by those local ground states simultaneously. So, if there is one $|w\rangle$ we know that $w_2 = +1$ because there is an even number of stars crossed by the Wilson loop and there can not be any $|\tilde{w}\rangle$ state changing the eigenvalue to -1. The analog argument holds true for w_1 if there is a $|\tilde{w}\rangle$ state in the system. So there can be no ground state in the symmetry sector $(-,-)$ since local ground states w and $\tilde{w}$ would be needed on the checkerboard. For a system with an uneven length L,

we find with the same arguments that all ground states are in the symmetry sectors $(-,-)$,$(+,-)$ and $(-,+)$ since the product w_i now has an odd number of -1 factors. All the symmetry sectors with ground states in the checkerboard $U(1)$ toric code are the ones with ground states in the $U(1)$ toric code for even and odd system size, as seen in Chapter 2.

IV.3 Perturbation theory applied to the checkerboard $U(1)$ toric code

In this section, the perturbative formalism first introduced by Takahashi in Ref. [28] is applied to the checkerboard $U(1)$ toric code. For this, we separate the Hamiltonian into two parts

$$H_{U(1)\mathrm{CB}} = H_0 + \lambda_{A''} V \tag{IV.11}$$

with

$$H_0 = -\lambda_B \sum_p B_p - \lambda_{A'} \sum_{s' \in S'} \tilde{A}_{s'} \tag{IV.12}$$

and

$$V = - \sum_{s'' \in S''} \tilde{A}_{s''}. \tag{IV.13}$$

To use degenerate perturbation theory, we then define P as the projector on the ground state manifold and $S = \frac{1-P}{E_0 - H}$, where E_0 is the unperturbed energy. Using Takahashis perturbative approach, the effective Hamiltonian in fourth order reads

$$H_{\mathrm{eff}} = H_0 + H_1 \lambda_{A''} + H_2 \lambda_{A''}^2 + H_3 \lambda_{A''}^3 + H_4 \lambda_{A''}^4 \tag{IV.14}$$

where

$$
\begin{aligned}
H_1 &= PVP, \\
H_2 &= PVSVP, \\
H_3 &= PVSVSVP + PVPVSSVP + PVSSVVP, \\
H_4 &= \frac{1}{2}PVPVPVSSSVP - \frac{1}{2}PVPVSVSSVP - \frac{1}{2}PVPVSSVSVP \\
&\quad -\frac{1}{2}PVSVPVSSVP + PVSVSVSVP \\
&\quad +\frac{1}{2}PVSSSVPVPVP - \frac{1}{2}PVSSVSVPVP \\
&\quad -\frac{1}{2}PVPVSSVSVP - \frac{1}{2}PVSSVPVSVP.
\end{aligned}
$$

Before constructing the effective Hamiltonian, we discuss the action of $\tilde{A}_s$ on states in the ground state manifold. As already mentioned before, acting with $\tilde{A}_s$ on a product state either flips all spins on the product or projects to 0. To see how the perturbation acts on a ground state of the unperturbed system, the local ground states that are influenced by the action of $\tilde{A}_s$ can be written in the σ^z product state basis

$$
|x_1, x_2, x_3, x_4\rangle = \left|\frac{a_1 + b_1}{\sqrt{2}}, \frac{a_2 + b_2}{\sqrt{2}}, \frac{a_3 + b_3}{\sqrt{2}}, \frac{a_4 + b_4}{\sqrt{2}}\right\rangle \tag{IV.15}
$$

where $|x_i\rangle$ are the local ground states of $\tilde{A}_i$ influenced by the perturbation $\tilde{A}_s$, $|a_i\rangle$ are $|0\rangle$, $|1\rangle$ or $|-1\rangle$, and b_i are the corresponding states $|\bar{0}\rangle$, $|\bar{1}\rangle$ or $|-\bar{1}\rangle$. Since $\tilde{A}_s$ either projects a product state to 0 or flips the spins, we find that the final state is a sum of states where the four spins the perturbation acted on are flipped. Since all local ground states are a sum of flippable stars, the product states resulting after one spin is flipped are eigenstates of $\tilde{A}_s$ to the eigenvalue 0. So acting with $\tilde{A}_s$ creates four exitations on the surrounding stars. This way, we can see that only even orders can contribute to the effective Hamiltonian for an infinite lattice, since every $\tilde{A}_s$ has to perturb the same star two times to result in a state that is not projected to 0 by P in Takahashi perturbation theory. But on an infinite system the only possibility to perturb every star twice is acting on every star twice with the perturbation $\tilde{A}_s$. With this one can deduce that all terms in IV.14 that contain PVP vanish in an infinite system.

The next impotent property is that unperturbed ground states do not couple in finite order. For two ground states to couple one would need L $\tilde{A}_s$ to act one a ground state since diagonals constraint to be w or $\tilde{w}$ have to be created or destroyed. So we know that the effective Hamiltonian only has diagonal corrections in any finite order. The question remains if one of the ground states is energetically preferred. It turns out that this is the case. The state where all local $\tilde{A}_s$ eigenstates are $|v\rangle$ is the energetically

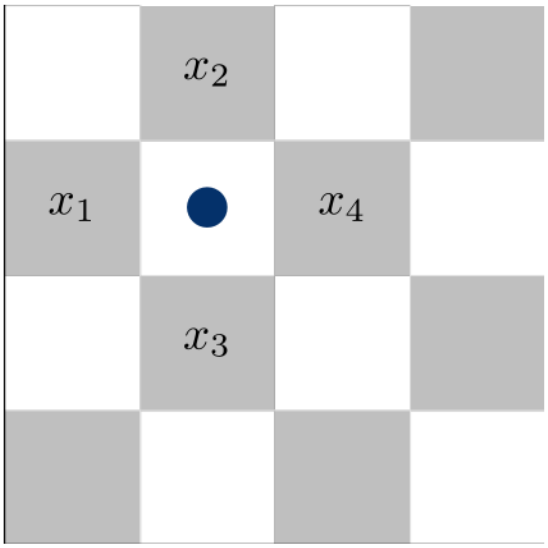

Figure IV.9: The blue dot is the star the perturbation acts on, the x_i give the convention for the order of the states $|x_1, x_2, x_3, x_4\rangle$

.

most favorable state. Even more interesting, the gap to the other ground states grows subextensively.

To show this we first calculate the second-order perturbation theory. Starting with a tensor product of the local ground state with the convention depicted in IV.9 and expanding into a product state, we obtain

$$|v, v, v, v\rangle = \frac{1}{\sqrt{2^4}} \sum_{i_1,i_2,i_3,i_4} |0_{i_1}, 0_{i_2}, 0_{i_3}, 0_{i_4}\rangle$$

where $0_1 = 0$ and $0_2 = \bar{0}$. Acting with $\tilde{A}_s$ on this state, we get

$$\tilde{A}_s |v, v, v, v\rangle = \frac{1}{\sqrt{2^4}}(|b, d, c, a\rangle + \left|\bar{b}, c, \bar{d}, a\right\rangle + \left|\bar{b}, \bar{c}, d, a\right\rangle + |b, \bar{c}, d, \bar{a}\rangle + \left|b, c, \bar{d}, \bar{a}\right\rangle + \left|\bar{b}, \bar{c}, \bar{d}, \bar{a}\right\rangle)$$

where the states correspond to the stars seen in Figure IV.5. Now all non flippable stars are local eigenvectors to the eigenvalue 0. So acting with S gives a factor $-1/4$ for all product states, and acting with $\tilde{A}_s$ on the same star flips all spins since none of the states are projected out again. As we have already seen, acting on a different star would give an excited state and would be projected out by P in order 2. With this, we

obtain

$$\tilde{A}_s S \tilde{A}_s \left|v,v,v,v\right\rangle =$$
$$\frac{1}{\sqrt{2^4}}\frac{1}{-4}(\left|0,0,0,0\right\rangle + \left|\bar{0},0,\bar{0},0\right\rangle + \left|\bar{0},\bar{0},0,0\right\rangle + \left|0,\bar{0},0,\bar{0}\right\rangle + \left|0,0,\bar{0},\bar{0}\right\rangle + \left|\bar{0},\bar{0},\bar{0},\bar{0}\right\rangle)$$

and can now calculate the diagonal matrix element

$$\left\langle v,v,v,v\right| \tilde{A}_s S \tilde{A}_s \left|v,v,v,v\right\rangle = -\frac{6}{2^6}. \tag{IV.16}$$

We notice that the calculation did not depend on the local ground states chosen on the checkerboard, even though we have done it for a concrete example, since every one of the local ground states is a superposition of product states, with one of them being spin up on the perturbation and one being spin down. This statement is also true for higher orders; if the perturbation acts only on one star next to an unperturbed star, the local ground state of this star does not change the matrix element.
Next, we calculate the perturbative corrections in order 4. We do this for a state with one diagonal restricted to $|w\rangle$ ground states and for a state with no diagonal restricted. We are only interested in the perturbative processes that differ for the ground states. So all processes where the perturbations affect the diagonals only once are not interesting. The remaining processes are the ones where the perturbations cross the diagonal, as seen in Figure IV.10 if x_3 and x_4 are restricted and IV.11, if x_3, x_4, and x_5 are restricted. Other processes acting on local ground states of the diagonal twice are processes acting parallel to the diagonal. Such a process does not change the matrix element since the spins shared by $|0\rangle$ and $|\bar{0}\rangle$ with the next parallel diagonal the perturbation acts on are the same the states $|1\rangle$ and $|\bar{1}\rangle$ share with the diagonal.

To calculate the corrections, we first consider processes depicted by stars acting like seen in Figure IV.10. We label the upper star s and the lower one s'. Since $\tilde{A}_s$ has to act twice on every star to get an overlap with a ground state in the final state, terms with a sequence PVP vanish. This leaves us with contributions from the operators $PVSVSVSVP$, $PVSVPVSSVP$ and $PVSSVPVSVP$. We argue that the diagonal matrix elements of the second and third ones do not depend on the states on the diagonal. First, we notice that all the residues S give a factor of $-1/4$ since they are acting on states perturbed once if the left ones act on the left state and the right ones on the right state. Then, since there are only diagonal corrections, we can write $P = \left|\mathrm{gs}\right\rangle \left\langle \mathrm{gs}\right|$ where $\left|\mathrm{gs}\right\rangle$ is the ground state of which we calculate the matrix element. So we obtain

$$\left\langle \mathrm{gs}\right| P\tilde{A}_{s'} S S \tilde{A}_{s'} P \tilde{A}_s S \tilde{A}_s P \left|\mathrm{gs}\right\rangle = \frac{-1}{4^3} \left\langle \mathrm{gs}\right| A_{s'}^2 \left|\mathrm{gs}\right\rangle \left\langle \mathrm{gs}\right| A_s^2 \left|\mathrm{gs}\right\rangle \tag{IV.17}$$

which is independent of the ground state $\left|\mathrm{gs}\right\rangle$. Contributions coming from the acting on star first and then on the second vanish all since such a state is always projected to

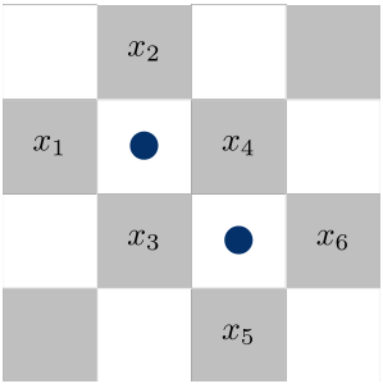

Figure IV.10: Convention used for processes in perturbation theory that act diagonally.

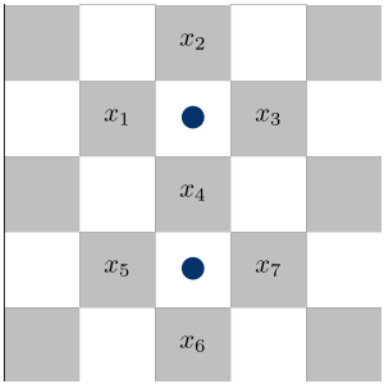

Figure IV.11: Convention used for processes in perturbation theory that act vertically.

0 by P.
So the only remaining contribution that can partially lift the degeneracy of the ground state is coming from the term $PVSVSVSVP$. First, we calculate the diagonal matrix element for a state with a diagonal constraint of $|w\rangle$. In our convention, this term is given by $|v,v,w,w,v,v\rangle$. As we have argued before, the states $|v\rangle$ could be different local ground states without changing the matrix element since they share only one spin with the stars the perturbations act on. We calculate

$$\begin{aligned}
\tilde{A}_{s'}S\tilde{A}_sS\tilde{A}_{s'}S\tilde{A}_sP\,|v,v,w,w,v,v\rangle &= \tilde{A}_{s'}S\tilde{A}_sS\tilde{A}_{s'}S\frac{1}{\sqrt{2^4}}(\left|b,\bar{d},\bar{c},a,v,v\right\rangle + \left|b,\bar{d},c,\bar{a},v,v\right\rangle \\
&+ |b,d,\bar{c},\bar{a},v,v\rangle + \left|\bar{b},\bar{d},c,a,v,v\right\rangle + \left|\bar{b},d,\bar{c},a,v,v\right\rangle + \left|\bar{b},d,c,\bar{a},v,v\right\rangle) = \\
&= \tilde{A}_{s'}S\tilde{A}_sS\frac{1}{-4}\frac{1}{\sqrt{2^4}}(\left|b,\bar{d},\bar{e},e,c,\bar{a}\right\rangle + \left|b,\bar{d},\bar{e},e,\bar{c},a\right\rangle + \left|b,\bar{d},e,\bar{e},c,\bar{a}\right\rangle \\
&+ \left|b,\bar{d},e,\bar{e},\bar{c},a\right\rangle + |b,d,\bar{e},\bar{e},c,a\rangle + \left|\bar{b},\bar{d},e,e,\bar{c},\bar{a}\right\rangle + \left|\bar{b},d,\bar{e},e,\bar{c},a\right\rangle \\
&+ \left|\bar{b},d,\bar{e},e,c,\bar{a}\right\rangle + \left|\bar{b},d,e,\bar{e},\bar{c},a\right\rangle) + \left|\bar{b},d,e,\bar{e},c,\bar{a}\right\rangle \\
&= \frac{1}{-4}\frac{1}{-6}\frac{1}{-4}\frac{1}{\sqrt{2^6}}(|0,0,1,1,0,0\rangle \\
&+ |0,\bar{0},1,\bar{1},\bar{0},0\rangle + |0,0,1,1,\bar{0},\bar{0}\rangle + |0,0,\bar{1},\bar{1},0,0\rangle \\
&+ |0,0,\bar{1},\bar{1},\bar{0},\bar{0}\rangle + |\bar{0},\bar{0},1,1,0,0\rangle + |\bar{0},\bar{0},1,1,\bar{0},\bar{0}\rangle \\
&+ |\bar{0},\bar{0},\bar{1},\bar{1},0,0\rangle + |\bar{0},\bar{0},\bar{1},\bar{1},\bar{0},\bar{0}\rangle + |\bar{0},0,\bar{1},1,0,\bar{0}\rangle)
\end{aligned}$$

Having calculated this, the diagonal matrix element is given as

$$\langle v,v,w,w,v,v|\, P\tilde{A}_{s'}S\tilde{A}_sS\tilde{A}_{s'}S\tilde{A}_sP\,|v,v,w,w,v,v\rangle = -\frac{1}{6}\frac{1}{4^2}\frac{10}{2^6}. \tag{IV.18}$$

Next, we calculate the matrix element for a ground state without a restricted diagonal. We do this for the state $|v,v,v,v,v,v\rangle$ but the outer $|v\rangle$ states can be changed to any other local ground state, and the ones in the middle that we act twice on can be changed to $|\tilde{w}\rangle$ states, since the spins $|0\rangle$ and $|\bar{0}\rangle$ share with the star the perturbation acts on are the same that $|-1\rangle$ and $|-\bar{1}\rangle$ share with them. So we calculate

$$\begin{aligned}
\tilde{A}_{s'}S\tilde{A}_sS\tilde{A}_{s'}S\tilde{A}_sP\,|v,v,v,v,v,v\rangle = \tilde{A}_{s'}S\tilde{A}_sS\tilde{A}_{s'}S\frac{1}{\sqrt{2^4}}(&\left|b,\bar{d},\bar{a},c,v,v\right\rangle + \left|b,\bar{d},a,\bar{c},v,v\right\rangle \\
+|b,d,\bar{a},\bar{c},v,v\rangle + \left|\bar{b},\bar{d},a,c,v,v\right\rangle &+ \left|\bar{b},d,\bar{a},c,v,v\right\rangle + \left|\bar{b},d,a,\bar{c},v,v\right\rangle) = \\
\tilde{A}_{s'}S\tilde{A}_sS\frac{1}{-4}\frac{1}{\sqrt{2^6}}(&\left|b,\bar{d},\bar{-1},-1,c,\bar{a}\right\rangle + \left|b,\bar{d},\bar{-1},-1,\bar{c},a\right\rangle + \left|b,\bar{d},-1,\bar{-1},c,\bar{a}\right\rangle \\
+\left|b,\bar{d},-1,\bar{-1},\bar{c},a\right\rangle &+ \left|\bar{b},\bar{d},\bar{-1},\bar{-1},c,a\right\rangle + |b,d,-1,-1,\bar{c},\bar{a}\rangle \\
+\left|\bar{b},d,\bar{-1},-1,\bar{c},a\right\rangle &+ \left|\bar{b},d,\bar{-1},-1,c,\bar{a}\right\rangle + \left|\bar{b},d,-1,\bar{-1},\bar{c},a\right\rangle + \left|\bar{b},d,-1,\bar{-1},c,\bar{a}\right\rangle)
\end{aligned}$$

To calculate S we need to make a change of basis in the eigenbasis of the Hamiltonian given as

$$|-1\rangle = \frac{|\tilde{w}\rangle + |\tilde{w}_-\rangle}{\sqrt{2}} \tag{IV.19}$$

and

$$|-\bar{1}\rangle = \frac{|\tilde{w}\rangle - |\tilde{w}_-\rangle}{\sqrt{2}}. \tag{IV.20}$$

From this, it follows:

$$|-1,\bar{-1}\rangle + |\bar{-1},-1\rangle = |\tilde{w},\tilde{w}\rangle - |\tilde{w}_-,\tilde{w}_-\rangle \tag{IV.21}$$

and we can continue calculating

$$\tilde{A}_{s'}S\tilde{A}_sS\frac{1}{-4}\frac{1}{\sqrt{2^6}}(\left|b,\bar{d},\tilde{w},\tilde{w},c,\bar{a}\right\rangle+\left|b,\bar{d},\tilde{w},\tilde{w},\bar{c},a\right\rangle-\left|b,\bar{d},\tilde{w}_-,\tilde{w}_-,c,\bar{a}\right\rangle$$
$$-\left|b,\bar{d},\tilde{w}_-,\tilde{w}_-,\bar{c},a\right\rangle+\left|\bar{b},\bar{d},\bar{-}1,\bar{-}1,c,a\right\rangle+|b,d,-1,-1,\bar{c},\bar{a}\rangle-\left|\bar{b},d,\tilde{w}_-,\tilde{w}_-,\bar{c},a\right\rangle$$
$$+\left|\bar{b},d,\tilde{w},\tilde{w},c,\bar{a}\right\rangle+\left|\bar{b},d,\tilde{w},\tilde{w},\bar{c},a\right\rangle)-\left|\bar{b},d,\tilde{w}_-,\tilde{w}_-,c,\bar{a}\right\rangle)=$$
$$\tilde{A}_{s'}S\tilde{A}_sS\frac{1}{-4}\frac{1}{\sqrt{2^6}}(\left|b,\bar{d},\tilde{w},\tilde{w},c,\bar{a}\right\rangle+\left|b,\bar{d},\tilde{w},\tilde{w},\bar{c},a\right\rangle-\left|b,\bar{d},\tilde{w}_-,\tilde{w}_-,c,\bar{a}\right\rangle$$
$$-\left|b,\bar{d},\tilde{w}_-,\tilde{w}_-,\bar{c},a\right\rangle-\left|\bar{b},d,\tilde{w}_-,\tilde{w}_-,\bar{c},a\right\rangle+\left|\bar{b},d,\tilde{w},\tilde{w},c,\bar{a}\right\rangle$$
$$+\left|\bar{b},d,\tilde{w},\tilde{w},\bar{c},a\right\rangle)-\left|\bar{b},d,\tilde{w}_-,\tilde{w}_-,c,\bar{a}\right\rangle+1/2(|b,d,\tilde{w},\tilde{w},\bar{c},\bar{a}\rangle+|b,d,\tilde{w},\tilde{w_-},\bar{c},\bar{a}\rangle$$
$$+|b,d,\tilde{w_-},\tilde{w},\bar{c},\bar{a}\rangle+|b,d,\tilde{w_-},\tilde{w_-},\bar{c},\bar{a}\rangle)+1/2(\left|\bar{b},\bar{d},\tilde{w},\tilde{w},c,a\right\rangle+\left|\bar{b},\bar{d},\tilde{w},\tilde{w_-},c,a\right\rangle$$
$$+\left|\bar{b},\bar{d},\tilde{w_-},\tilde{w},c,a\right\rangle+\left|\bar{b},\bar{d},\tilde{w_-},\tilde{w_-},c,a\right\rangle))$$

This gives the result for the matrix element

$$\langle v,v,v,v,v,v|\,P\tilde{A}_{s'}S\tilde{A}_sS\tilde{A}_{s'}S\tilde{A}_sP\,|v,v,v,v,v,v\rangle=-\frac{1}{4^2}\frac{1}{2^6}(\frac{4}{4}+\frac{4}{8}+\frac{1}{4}(\frac{2}{4}+\frac{2}{8}+\frac{4}{6})).$$

The contribution of processes equivalent to the one seen in Figure IV.11 is calculated to

$$\tilde{A}_{s'}S\tilde{A}_sS\tilde{A}_{s'}S\tilde{A}_s\,|v,v,v,v,v,v,v,v\rangle=\tilde{A}_{s'}S\tilde{A}_sS\tilde{A}_{s'}S\tfrac{1}{\sqrt{2^4}}(\left|b,\bar{d},\bar{a},c,v,v,v\right\rangle$$
$$+\left|b,\bar{d},a,\bar{c},v,v,v\right\rangle+|b,d,\bar{a},\bar{c},v,v,v\rangle+\left|\bar{b},\bar{d},a,c,v,v,v\right\rangle+\left|\bar{b},d,\bar{a},c,v,v,v\right\rangle+\left|\bar{b},d,a,\bar{c},v,v,v\right\rangle)=$$

$$\tilde{A}_{s'}S\tilde{A}_sS\tfrac{1}{-4}\tfrac{1}{\sqrt{2^7}}(\left|b,\bar{d},\bar{a},e,b,\bar{c},\bar{a}\right\rangle+\left|b,\bar{d},\bar{a},e,\bar{b},c,\bar{a}\right\rangle+\left|b,\bar{d},\bar{a},e,\bar{b},\bar{c},a\right\rangle+\left|\bar{b},\bar{d},a,e,b,\bar{c},\bar{a}\right\rangle$$
$$+\left|\bar{b},\bar{d},a,e,\bar{b},c,\bar{a}\right\rangle+\left|\bar{b},\bar{d},a,e,\bar{b},\bar{c},a\right\rangle+\left|\bar{b},d,\bar{a},e,b,\bar{c},\bar{a}\right\rangle+\left|\bar{b},d,\bar{a},e,\bar{b},c,\bar{a}\right\rangle+\left|\bar{b},d,\bar{a},e,\bar{b},\bar{c},a\right\rangle$$
$$+\left|b,\bar{d},a,\bar{e},b,c,\bar{a}\right\rangle+\left|b,\bar{d},a,\bar{e},b,\bar{c},a\right\rangle+\left|b,\bar{d},a,\bar{e},\bar{b},c,a\right\rangle+|b,d,\bar{a},\bar{e},b,c,\bar{a}\rangle$$
$$+|b,d,\bar{a},,\bar{e},b,\bar{c},a\rangle+\left|b,d,\bar{a},,\bar{e},\bar{b},c,a\right\rangle+\left|\bar{b},d,a,\bar{e},b,c,\bar{a}\right\rangle+\left|\bar{b},d,a,\bar{e},b,\bar{c},a\right\rangle+\left|\bar{b},d,a,\bar{e},\bar{b},c,a\right\rangle$$
$$=\tfrac{1}{4^2}\tfrac{-1}{7}\tfrac{1}{2^7}(|0,\bar{0},\bar{0},0,0,\bar{0},\bar{0}\rangle+|0,\bar{0},\bar{0},0,\bar{0},0,\bar{0}\rangle+|0,\bar{0},\bar{0},0,\bar{0},\bar{0},0\rangle$$
$$+|\bar{0},\bar{0},0,0,0,\bar{0},\bar{0}\rangle+|\bar{0},\bar{0},0,0,\bar{0},0,\bar{0}\rangle+|\bar{0},\bar{0},0,0,\bar{0},\bar{0},0\rangle$$
$$+|\bar{0},0,\bar{0},0,0,\bar{0},\bar{0}\rangle+|\bar{0},0,\bar{0},0,\bar{0},0,\bar{0}\rangle+|\bar{0},0,\bar{0},0,\bar{0},\bar{0},0\rangle$$
$$+|0,\bar{0},0,\bar{0},0,0,\bar{0}\rangle+|0,\bar{0},0,\bar{0},0,\bar{0},0\rangle+|0,\bar{0},0,\bar{0},\bar{0},0,0\rangle$$
$$+|0,0,\bar{0},\bar{0},0,0,\bar{0}\rangle+|0,0,\bar{0},,\bar{0},0,\bar{0},0\rangle+|0,0,\bar{0},,\bar{0},\bar{0},0,0\rangle$$
$$+|\bar{0},0,0,\bar{0},0,0,\bar{0}\rangle+|\bar{0},0,0,\bar{0},0,\bar{0},0\rangle+|\bar{0},0,0,\bar{0},\bar{0},0,0\rangle)$$

We obtain the matrix element

$$\langle v,v,v,v,v,v,v|\,\tilde{A}_{s'}S\tilde{A}_sS\tilde{A}_{s'}S\tilde{A}_sP\,|v,v,v,v,v,v,v\rangle = -18\frac{1}{4^2\cdot 7}\frac{1}{2^7}. \tag{IV.22}$$

The same calculation for a state with a constraint diagonal is given by $|v,v,w,w,w,v,v\rangle$

$$\begin{aligned}
&\mathrm{P}\ \tilde{A}_{s'}S\tilde{A}_sS\tilde{A}_{s'}S\tilde{A}_sP\,|v,v,w,w,w,v,v\rangle = \\
&\tilde{A}_{s'}S\tilde{A}_sS\tilde{A}_{s'}S\tfrac{1}{\sqrt{2^4}}(\left|b,\bar{d},\bar{c},a,w,v,v\right\rangle + \left|b,\bar{d},c,\bar{a},w,v,v\right\rangle + |b,d,\bar{c},\bar{a},w,v,v\rangle \\
&+ \left|\bar{b},\bar{d},c,a,w,v,v\right\rangle + \left|\bar{b},d,\bar{c},a,w,v,v\right\rangle + \left|\bar{b},d,c,\bar{a},w,v,v\right\rangle) = \\
&\tilde{A}_{s'}S\tilde{A}_sS\tfrac{1}{-4}\tfrac{1}{\sqrt{2^7}}(\left|b,\bar{d},c,-1,b,\bar{c},\bar{a}\right\rangle + \left|b,\bar{d},c,-1,\bar{b},c,\bar{a}\right\rangle + \left|b,\bar{d},c,-1,\bar{b},\bar{c},a\right\rangle \\
&+ \left|\bar{b},d,c,-1,b,\bar{c},\bar{a}\right\rangle + \left|\bar{b},d,c,-1,\bar{b},c,\bar{a}\right\rangle + \left|\bar{b},d,c,-1,\bar{b},\bar{c},a\right\rangle \\
&+ |b,d,\bar{c},-1,b,\bar{c},\bar{a}\rangle + \left|b,d,\bar{c},-1,\bar{b},c,\bar{a}\right\rangle + \left|b,d,\bar{c},-1,\bar{b},\bar{c},a\right\rangle \\
&+ \left|\bar{b},\bar{d},c,\bar{-}1,b,c,\bar{a}\right\rangle + \left|\bar{b},\bar{d},c,\bar{-}1,b,\bar{c},a\right\rangle + \left|\bar{b},\bar{d},c,\bar{-}1,\bar{b},c,a\right\rangle \\
&+ \left|\bar{b},d,\bar{c},\bar{-}1,b,c,\bar{a}\right\rangle + \left|\bar{b},d,\bar{c},,\bar{-}1,b,\bar{c},a\right\rangle + \left|\bar{b},d,\bar{c},\bar{-}1,\bar{b},c,a\right\rangle \\
&+ \left|b,\bar{d},\bar{c},\bar{-}1,b,c,\bar{a}\right\rangle + \left|b,\bar{d},\bar{c},\bar{-}1,b,\bar{c},a\right\rangle + \left|b,\bar{d},\bar{c},\bar{-}1,\bar{b},c,a\right\rangle)
\end{aligned}$$

Now we can again change the basis to calculate S

$$\begin{aligned}
&\tilde{A}_{s'}S\tilde{A}_sS\tfrac{1}{-4}\tfrac{1}{\sqrt{2^7}}(\left|b,\bar{d},c,\tfrac{|w\rangle+|w_-\rangle}{\sqrt{2}},b,\bar{c},\bar{a}\right\rangle+\left|b,\bar{d},c,\tfrac{|w\rangle+|w_-\rangle}{\sqrt{2}},\bar{b},c,\bar{a}\right\rangle+\left|b,\bar{d},c,\tfrac{|w\rangle+|w_-\rangle}{\sqrt{2}},\bar{b},\bar{c},a\right\rangle \\
&+ \left|\bar{b},d,c,\tfrac{|w\rangle+|w_-\rangle}{\sqrt{2}},b,\bar{c},\bar{a}\right\rangle + \left|\bar{b},d,c,\tfrac{|w\rangle+|w_-\rangle}{\sqrt{2}},\bar{b},c,\bar{a}\right\rangle + \left|\bar{b},d,c,\tfrac{|w\rangle+|w_-\rangle}{\sqrt{2}},\bar{b},\bar{c},a\right\rangle \\
&+ \left|b,d,\bar{c},\tfrac{|w\rangle+|w_-\rangle}{\sqrt{2}},b,\bar{c},\bar{a}\right\rangle + \left|b,d,\bar{c},\tfrac{|w\rangle+|w_-\rangle}{\sqrt{2}},\bar{b},c,\bar{a}\right\rangle + \left|b,d,\bar{c},\tfrac{|w\rangle+|w_-\rangle}{\sqrt{2}},\bar{b},\bar{c},a\right\rangle \\
&+ \left|\bar{b},\bar{d},c,\tfrac{|w\rangle-|w_-\rangle}{\sqrt{2}},b,c,\bar{a}\right\rangle + \left|\bar{b},\bar{d},c,\tfrac{|w\rangle-|w_-\rangle}{\sqrt{2}},b,\bar{c},a\right\rangle + \left|\bar{b},\bar{d},c,\tfrac{|w\rangle-|w_-\rangle}{\sqrt{2}},\bar{b},c,a\right\rangle \\
&+ \left|\bar{b},d,\bar{c},\tfrac{|w\rangle-|w_-\rangle}{\sqrt{2}},b,c,\bar{a}\right\rangle + \left|\bar{b},d,\bar{c},,\tfrac{|w\rangle-|w_-\rangle}{\sqrt{2}},b,\bar{c},a\right\rangle + \left|\bar{b},d,\bar{c},\tfrac{|w\rangle-|w_-\rangle}{\sqrt{2}},\bar{b},c,a\right\rangle \\
&+ \left|b,\bar{d},\bar{c},\tfrac{|w\rangle-|w_-\rangle}{\sqrt{2}},b,c,\bar{a}\right\rangle + \left|b,\bar{d},\bar{c},\tfrac{|w\rangle-|w_-\rangle}{\sqrt{2}},b,\bar{c},a\right\rangle + \left|b,\bar{d},\bar{c},\tfrac{|w\rangle-|w_-\rangle}{\sqrt{2}},\bar{b},c,a\right\rangle).
\end{aligned}$$

So we obtain the matrix element

$$\langle v,v,w,w,w,v,v|\,P\tilde{A}_{s'}S\tilde{A}_sS\tilde{A}_{s'}S\tilde{A}_sP\,|v,v,w,w,w,v,v\rangle = -\frac{1}{4^2}\frac{1}{2^7}\frac{1}{2}(\frac{18}{6}+\frac{18}{8})$$

Processes like $P\tilde{A}_{s'}S\tilde{A}_{s'}S\tilde{A}_sS\tilde{A}_s$ where the first star is acted on twice and then on the second star were not discussed yet, but it turns out that these processes give the same contribution independent of the local ground states of the neighboring stars. Calculating the matrix element gives

$$\langle \mathrm{gs}|\, \tilde{A}_{s'}S\tilde{A}_{s'}S\tilde{A}_sS\tilde{A}_s\, |\mathrm{gs}\rangle = \frac{1}{4^2}\langle \mathrm{gs}|\, \tilde{A}^2_{s'}S\tilde{A}^2_s\, |\mathrm{gs}\rangle = \frac{-1}{4^3}\sum_i S_i \langle i|\, \tilde{A}^2_s\, |\mathrm{gs}\rangle \langle i|\, \tilde{A}^2_{s'}\, |\mathrm{gs}\rangle^*$$

with $S_i = \langle i|\, S\, |i\rangle$ and the sum running over all excited states $|i\rangle$. But as seen before in the second order calculation, when calculating A^2_s the local ground states are interchangeable for this calculation, and the same holds true for this one. All matrix elements that contribute to the difference in energy for the ground states in order 4 have been calculated. The energy difference is given by

$$\begin{aligned} E_v - E_{\mathrm{diag}} = 4L(-\frac{1}{4^2}\frac{1}{2^6}(\frac{4}{4}+\frac{4}{8}+\frac{1}{4}(\frac{2}{4}+\frac{2}{8}+\frac{4}{6}))+\frac{1}{6}\frac{1}{4^2}\frac{10}{2^6} \\ -\frac{18}{4^2}\frac{1}{7}\frac{1}{2^6}+\frac{1}{4^2}\frac{1}{2^6}\frac{1}{2}(\frac{18}{6}+\frac{18}{8}))\lambda^4_{A''}+O(\lambda^6_{A''}), \end{aligned} \quad \text{(IV.23)}$$

where E_v is the state where all local ground states are put to $|v\rangle$ and E_{diag} is the state where all local ground states are $|v\rangle$ but one diagonal is restricted to be $|w\rangle$. The matrix element for the last two terms has been multiplied by 2 since there are double the number of processes seen in Figure IV.11 than seen in Figure IV.10 and the factor 4 comes from the different ways one can distribute the stars in the contributing operators. The value for the term IV.23 is $-1.30789621 \times 10^{-4}$, this is a negative value, which shows that in order 4 the state E_v is the global ground state. The linear dependence on the length shows that the gap grows subextensively and is infinite in the thermodynamic limit.

IV.4 Fractons as elementary excitations

In the last section, we have seen how, in fourth-order perturbation theory, one ground state is selected to be the global ground state. The other states in the ground-state manifold acquire a gap of order L. In this section, the states that have a gap of $O(1)$ are discussed, and confined fractons are found.

Fractons were only discovered rather recently. The first paper with fractonic excitations was Ref. [29] published by Claudio Chamon in 2005, in which an exactly solvable 3D topologically-ordered spin model was constructed, which was then shown to feature glassy dynamics, i.e. the system does reach thermal equilibrium much slower than ordinary systems. The Chamon model is a model hosting type 1 fractons. This type of fractons cannot move in isolation, but composite fractons are mobile again. In his work

published in 2011 [30], looking for a system with stable quantum memory, Jeongwan Haah found a 3D model with completely immobile excitations. Even composite fractons cannot move in this model. These fractons are called type 2 fractons. In 2016, Sagar Vijay, Jeongwan Haah, and Liang Fu put fractons in the context of generalized lattice gauge theories [31] and coined the term fracton. Shortly after this, Michael Pretko discussed higher rank symmetric $U(1)$ tensor gauge theories as a possible phase in spin liquids and found using a generalized Gauß law that the matter field such a gauge theory couples to have to host particles with restricted mobility [32]. This fracton model is a gapless fracton phase. Since then, a lot of research has been done on systems hosting fractons. There are a lot of new interesting phenomena to study in such systems, for example, new hydrodynamic classes with sub diffusive behavior [33], the mentioned glassy dynamics [29, 34], relations to classical and quantum elasticity theory [35, 10], connections to gravity [10, 36], and the search for phase transitions outside of the Landau Wilson Ginsburg paradigm [37, 38, 39]. On the experimental side, progress is made as well. Recently, for example, fractons were studied on a quantum simulator in Ref. [40]. Although the gapped topologically ordered fracton phases have not been seen in experiments, there are some proposals to engineer such phases using, for example, a symmetry principle called combinatorial gauge symmetry [7]. Also, the introduction of the $U(1)$ toric code was in part motivated by combinatorial gauge symmetry [9].
First, we list all the elementary excitations with a gap of $O(1)$ in the system size. There are three types of excitation: plaquette excitations, which are created by the violation of the constraint $B_p |\Psi\rangle = |\Psi\rangle$, star excitations with eigenvalue 0, and star excitations with eigenvalue -1 on the global ground state. We will see that the excitations corresponding to the star eigenvalue -1 are not fractons. The ones corresponding to a violation of the constraint $B_p |\Psi\rangle = |\Psi\rangle$ behave like lineons, and the ones corresponding to the eigenvalue 0 for the star operator are fractons. The local excited states with eigenvalue 0 can be seen in Figure IV.5.

IV.5 Plaquette excitations

The plaquette excitations are created if the constraint $B_p |\Psi\rangle = |\Psi\rangle$ is violated. This means that if we expand the excited state in the σ^z product state basis, every product state has to share an odd number of $|\uparrow\rangle$ and $|\downarrow\rangle$ with the excited plaquette. If we now require that all the states of the unperturbed stars are local ground states, we again find, that in the σ^z product state basis, the state with only plaquette excitations has to be a sum of product states built by flippable states on the unperturbed squares of the checkerboard IV.3. Looking at the flippable stars and product states built up by those, we find that a plaquette excitation that sits on a diagonal of the unperturbed checker board restricts exactly one of the neighboring stars to be $|1\rangle$ or $|\bar{1}\rangle$ and for

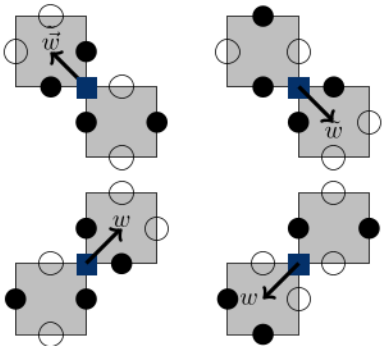

Figure IV.12: Plaqette excitation constrains exactly one of the neighbouring stars to be $|w\rangle$ or $|\tilde{w}\rangle$ a empty square stands for the local ground state $|v\rangle$

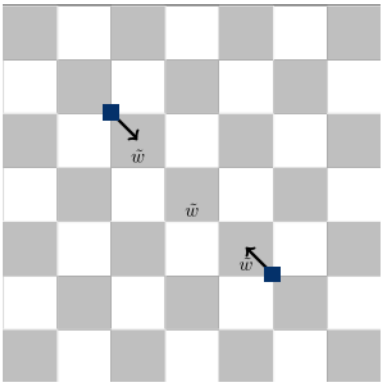

Figure IV.13: On the checkerboard, the lineons will be visualized by arrows, as seen in this picture.

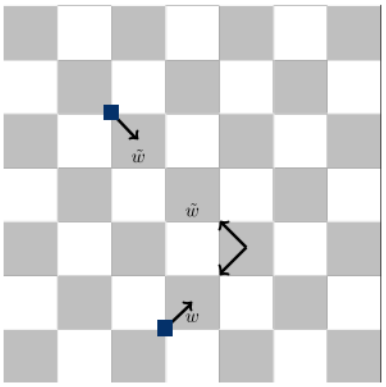

Figure IV.14: Lineons on different diagonals require star fractons to exist.

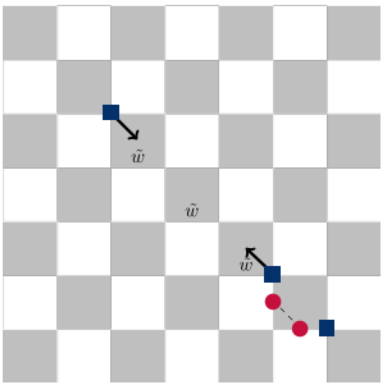

Figure IV.15: Lineons can move by acting wit σ^x on the red dots.

a plaquette excitation on the anti-diagonal it restricts exactly one of the stars to be either in the state $|-1\rangle$ or $|\bar{-1}\rangle$ as seen in Figure IV.14. Like in the chapters before, we can deduce now that exactly one of the states neighboring the plaquette excitation on the diagonal has to be in the state $|\tilde{w}\rangle$ and exactly one state neighboring a plaquette excitation on the anti-diagonal has to be $|w\rangle$. If we require only plaquett excitations on the torus and no star excitations, the diagonal has to be interrupted by another plaquette excitation otherwise, the diagonal would wind around the torus and meet the plaquette excitation again. But we found that exactly one state neighboring the plaquette is restricted to be $|w\rangle$ or $|\tilde{w}\rangle$ and not both, so this would be a contradiction. We find that two plaquett excitations on the same diagonal are enough to construct an excited state without leading to a contradiction. Now we investigate the mobility of such excitations on the ground state. We see that we can move the plaquette excitation diagonally by acting with σ^x matrices on the $|v\rangle$ state neighboring the plaquette so that the plaquette excitation moves on the diagonal and the $|v\rangle$ state is changed to a $|w\rangle$ state if the particle is moved along an anti-diagonal or $|\tilde{w}\rangle$ state if it is moved across the diagonal. This way, we increase the length of the string of $|w\rangle$ at the end of which the excitations are placed. The reverse process is possible as well. This moves the excitation along a one dimensional subspace. If we move the excitation orthogonal to the diagonal, we always have to create star or plaquette excitations. So we find that plaquette excitations are lineons.

IV.6 Fractonic star excitations

To discuss fractons, we change the basis in a suitable way. We do this by defining new excited states

$$
\begin{aligned}
|f_{\pm,1}\rangle &= (|a\rangle \pm |\bar{a}\rangle)) \\
|f_{\pm,2}\rangle &= (|b\rangle \pm |\bar{b}\rangle) \\
|f_{\pm,3}\rangle &= (|c\rangle \pm |\bar{c}\rangle) \\
|f_{\pm,4}\rangle &= (|d\rangle \pm |\bar{d}\rangle) \\
|f_{\pm,5}\rangle &= (|e\rangle \pm |\bar{e}\rangle)
\end{aligned}
$$

which all have an eigenvalue 0. We visualize these states on the checkerboard, as seen in Figure IV.16.
If we restrict the excited states to states with only this kind of excitation, so the constraint $B_p |\Psi\rangle = |\Psi\rangle$ cannot be violated, the same argument for the constraint in

Figure IV.4 holds. We find that an excited state depicted like in Figure IV.16 requires a state w or $\tilde{w}$ or an excited state in the direction the arrow is pointing. With this argument, we find that there are no local eigenstates with an eigenvalue 0 that can exist in isolation on the torus. The diagonal and anti-diagonal are constraint to be $|\tilde{w}\rangle$ and $|w\rangle$ meet at some point. This gives a contradiction to the requirement that no other local excitation is found on the checkerboard.
With this, we find that the diagonal and anti-diagonal have to be interrupted by another state with an eigenvalue 0. We also require that there is no restricted diagonal winding around the torus since then the state would again have a gap of $O(L)$. This then shows us that the lowest number of star fracton excitations on the torus is 4 excitations on the edges of a rectangle. Higher fracton number excitations are all the ones that can be created on the edges of a polygon with only right angles, where all the lines of the polygon are diagonals of the checkerboard. With the $|f_{+,5}\rangle$ state, more polygons sharing edges are possible excitations.
We discuss the mobility of these excitations. We restrict ourselves to the eigenstates $|f_{+,i}\rangle$, since we find $\sigma^z |f_{-,i}\rangle = \pm |f_{+,i}\rangle$, so if we can move $|f_{+,i}\rangle$ states by local operators, we can do the same with $|f_{-,i}\rangle$ just by acting with σ^z on those states before. If a star excitation in isolation sits on the checkerboard with an open boundary condition like seen in Figure IV.15 moving the excitation acting just with local operators around the excitation is impossible, since moving the particle to another state with only one excitation would require a whole diagonal or anti-diagonal to move. An excitation composite of two star fractons with the diagonal between them being constrained can move on a one-dimensional diagonal since, only for separating the excitations, a whole diagonal needs to be changed. Moving such fracton excitations can be done by acting with σ^x matrices along a rectangular path. A excitation composite of 4 fractons on a rectangle with a diagonal between the constraint can be moved freely by acting with σ^x operators. This is a typical behavior for type 1 fractons.
We briefly look at the relationship between plaquette excitations and star fractons. The plaquette excitations can move on diagonals, but when we move them orthogonal to the restricted diagonal they create a star fracton. So if we create two plaquette excitation move one around a rectangle with diagonals of the checkerboard as sides and than annihilate them again we have created four star fractons on the edges of the rectangle. This can be seen in Figure IV.19. We can also interpret moving the composite star fractons by creating two plaquette excitations and moving them on the restricted (anti)-diagonal so that all the $|w\rangle$ or $|\tilde{w}\rangle$ states are changed to $|v\rangle$ states, anihilating the star fracton on the edge of the rectangle, moving the plaqette excitation along the other restricted diagonal, and annihilating them again by creating a fracton and a restricted diagonal.

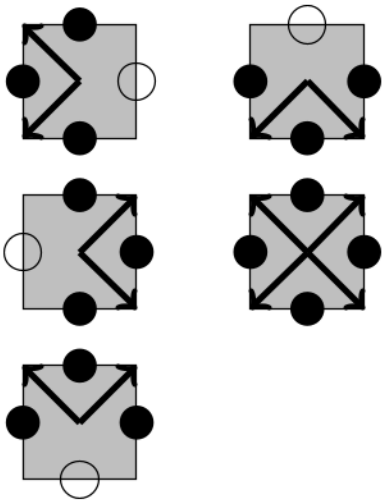

Figure IV.16: The fractons given by $|f_{i,+}\rangle$ are visualized by arrows on the checkerboard. The spins show an example of a product state, which is part of the superposition.

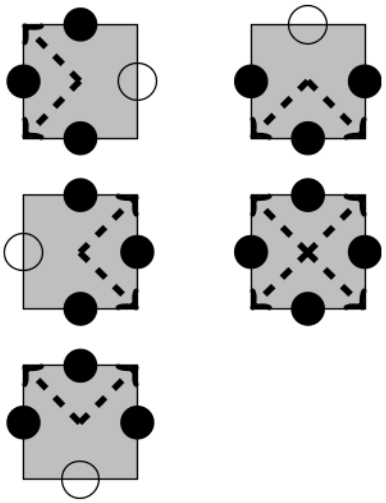

Figure IV.17: For completeness, there are five more fracton states on the checkerboard given by $|f_{i,-}\rangle$.

IV.7 Non fractonic excitations

The last type of excitation are $|v_-\rangle$, $|w_-\rangle$, and $|\tilde{w}_-\rangle$. These can be calculated by acting with σ^z on any site of a local ground state. They show no fractonic behavior since they can easily be moved by acting with σ^z matrices.

IV.8 Confinement

Another important property is that the diagonals are restricted to be $\tilde{w}$ or w cost energy, as seen in perturbation theory. We can deduce from this that the energy of an excited state with fractons grows linearly with distance if the fractons are separated. This property is called confinement and is well known for quarks in quantum chromodynamics [41]. But also for spin liquids, this property is not new. The polarized phase in the toric code in a magnetic field can be interpreted as a phase of confined and condensed anyons [42]. For some fracton models in a magnetic field in the polarized phase, this is the case as well [31].

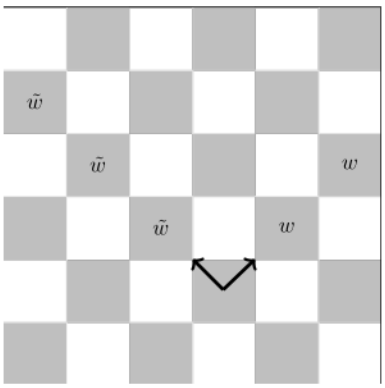

Figure IV.18: A fracton in isolation with open boundary condition. On an infinite lattice, the energy would grow with $O(L)$ and would not be an elementary excitation.

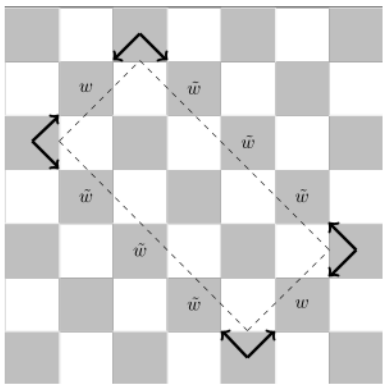

Figure IV.19: Four fractons created on the edges of a rectangle. The dashed line visualizes a string of σ^x matrices.

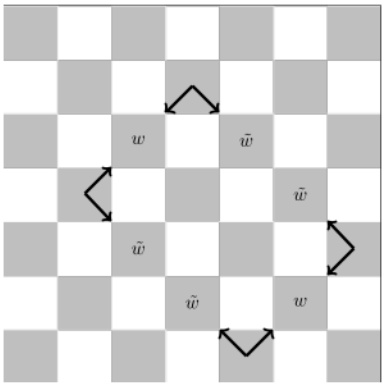

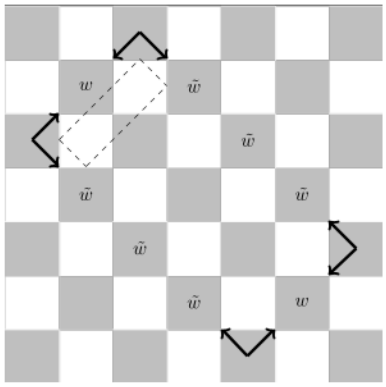

Figure IV.20: Moving fractons by acting with a closed rectangle of σ^x operators.

IV.9 ED results

In Figure IV.21 ED results for the two lowest energies are plotted for different $\lambda_{A''}$. We find a threefold ground-state degeneracy for $\lambda_{A''} = 0$ in the $(+,+)$ symmetry sector and a fourfold degeneracy for the $(-,-)$ symmetry sector. This adds up to $7 = 2^3 - 1$, consistent with the previous result. The ground state energies for $\lambda_{A''} = 1$ are 9.242 for the $(-,-)$ symmetry sector and 9.171 for the $(+,+)$ symmetry sector. This is the same result obtained in [9]: the topological ground state degeneracy was only found for larger system sizes with QMC. The kinks in the excited state come from a higher energy state crossing the state. We do not see the gap that opens in perturbation theory. This is not unexpected since the gap opens only at order four. The ED was done for a system with $L = 4$ so the ground states already couple in order four. No higher energy state crosses the ground state. This may indicate that no phase transition occurs and that the phase of the checkerboard $U(1)$ toric code is adiabaticaly connected to the one of the $U(1)$ toric code. This would be in contradiction to the suggested topological order in the $U(1)$ toric code [9]. In general, one cannot come to conclusions regarding the phase transition since the system size is too small and a lot of features of the phase were only found for larger system sizes in Ref. [9].

IV.10 Discussion

The phase found for small $\lambda_{A''}$ is not topological, as we do not find a ground state degeneracy or anyonic statistics. But looking at the low-energy excitations, i.e. the excitation with a gap of $O(1)$ in system size, we find that the excitations behave as fractons and lineons. The excitations are confined, so the real low energy excitations are bound states of these fractons. This opens the possibility of a phase transition similar to the one of the toric code in a magnetic field [42] or fractons in a magnetic field [31] where one finds one type of the topological excitations to be confined in the polarized phase because the phase is not topological and can not host topological excitations as "true" deconfined low energy excitations. Although there is work that claims that deconfined toplogical order fractons are impossible in 2D [43], 2D system with fracton topological order still have been found [44]. In the next chapter, we will argue that the plaquette excitations may still be good quasi particles in the $U(1)$ toric code phase and may still behave like fractons. For the calculated series expansion up to order four, the global ground state is in the symmetry sector $(+,+)$ for both compactifications and even system size L. All the ground states in the other symmetry sectors have at least one restricted diagonal, which leads to a gap of $O(L)$. For the topological phase, the ground states in the symmetry sectors that contribute to the ground-state manifold have to get lower in energy until they match the one of the global ground state. Another possibility is that the gap between the ground states

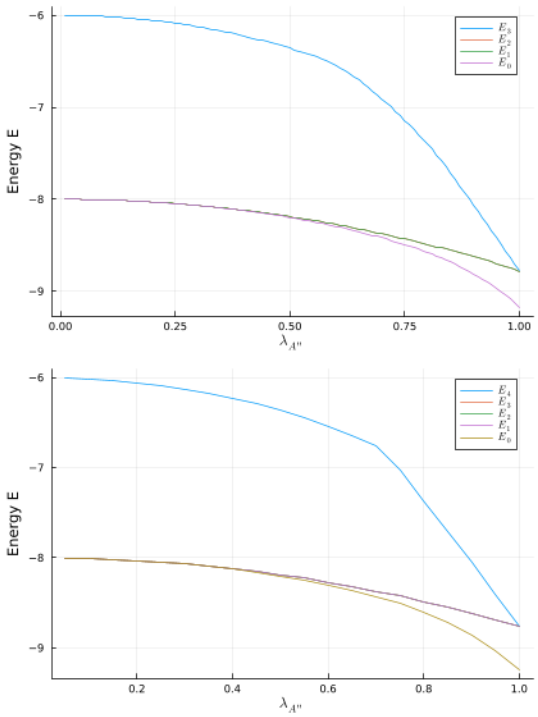

Figure IV.21: ED results for $\lambda_{A'} = 1$ $\lambda_B = 0$ in the symmetry sector with the eigenvalue of B_p equal to 1 and system size $L = 4$ and with $0°$ compactification. The upper plot shows the four lowest energy states in the $(+,+)$ sector, and the lower one shows the 4 lowest energy states in the $(-,-)$ symmetry sector.

in the checkerboard $U(1)$ toric code indeed persists to the $U(1)$ toric code model but was not detected. The largest system size the ground-state energy was calculated for is $L = 16$. The gap calculated in order 4 is still small for this system size and would have been inside the error bars of their QMC study.

V Fractons in the $U(1)$ toric code

In this section, the full original $U(1)$ toric code is discussed in a small magnetic field. Exact diagonalization (ED) is used to study different excited states of the $U(1)$ toric code, and how a small magnetic field would act on these states is discussed. We find signatures of fractonic behavior.

V.1 U(1)-toric code in a magnetic field

We first assume that the plaquette excitations can still be considered as quasi-particles. To see if the plaquette excitatations still behave as fractons, we consider the Hamiltonain $H_{U(1)}$ as defined in Equation III.4 under the action of a magnetic field.

$$H_{U(1),\text{mag}} = H_{U(1)} + h\sum_i \sigma_i^x \tag{V.1}$$

with $\lambda_B \gg \lambda_A \gg h$. Under this condition, the magnetic field can be seen as a perturbation to the unperturbed Hamiltonian.

To see if the plaquette excitations still behave like fractons or lineons, we have to analyze how fractons and lineons would behave under the action of a small magnetic field. A lineon could only move along the diagonal, so acting with 2 σ_i^x in perturbation theory on spins that would move the particle on a diagonal would give a state with the same energy in the thermodynamic limit. On a finite-size system and for dressed quasi-particles, this would, of course, not be true exactly. If the perturbative process is moving the particle out of the diagonal, we would find that an other excitation is created. So for our system, we do not know how the other quasi-particle excitation would look, but we could still see that the state after the action of σ^x is higher in energy. In general, since having two lineons not on a diagonal is not possible without fracton excitations as seen in Figure IV.14, we would expect the ground state in a symmetry sector with particles not placed on a diagonal to be higher in energy. We will discuss how the action of σ^x should influence type 1 fractons similar to the star excitations discussed in Chapter 4. This would be the case if they can only be placed on a rectangle with the diagonals as sides if one requires no other fractons. In this case, moving the particle in isolation should always give a higher energy state. Only moving the fractons in combination by acting σ^x should be possible without giving a

higher energy state. And we would also expect, that the ground state in a symmetry sector where the excitations are fixed in a way that different fracton excitations are necessary would have higher energy. In Figure V.6 we can see examples for this behavior. Subfigures b and c are examples for configurations that would be allowed for fractons, since all exitations are placed on the corners of a rectangle and all other subfigures show configurations where other fractons would be needed. With these considerations, we can now see if the plaquette excitations show signs of such behavior.

We investigate a system of size 4×4 with periodic boundary conditions in the $0°$ compactification using ED. We calculate the ground states for different symmetry sectors where some B_p eigenvalues were put to -1. We choose $\lambda_B = 0$ and $\lambda_A = 1$.

V.2 Results for ED with two particles

Already in the ground state energy for different symmetry sectors, an interesting behavior is found, as seen in Figure V.2. The ground state energies for symmetry sectors where the plaquett excitations were placed on a diagonal are lower and differ by at most 0.07. The ones where the excitations were placed not on a diagonal differed from the ones on the diagonal by at most 0.5 and by at most 0.28 from each other. This may indicates that moving the plaquette excitation out of the diagonal costs energy, and only moving it along the diagonal may energetically not be punished. Of course all the results have to be taken with caution since, for ED only small system sizes can be calculated and finite size effects play an important role. But this can still be seen as a hint that the excitations in the $U(1)$ toric code behave like fractons as well.

To get further indication if the excitations in the $U(1)$ toric code behave like fractons, we calculate the overlap between the ground state in a symmetry sector and a state moved by the perturbation

$$M = \left\langle \mathrm{gs}_{c,d} \right| \prod_i \sigma_i^x \left| \mathrm{gs}_{a,b} \right\rangle \tag{V.2}$$

where $\left|\mathrm{gs}_{x,y}\right\rangle$ is the ground state in the symmetry sector, with the plaquette operators on site x and y giving the eigenvalue -1. $\prod_i \sigma_i^x \left|\mathrm{gs}_{a,b}\right\rangle$ is a state where plaquette excitations were moved created and annihilated and $\left|\mathrm{gs}_{c,d}\right\rangle$ is the ground state in the symmetry sector the state was moved to. We only look at those where plaquette excitations were only moved. For lineons, we expect this overlap to be large for transitions where no other particle is created. In Figure V.3 the overlap was calculated for some examples. The processes in subfigures a and b are the ones we expect to be large if the plaquette excitations are lineons. Indeed, we find that this is the case

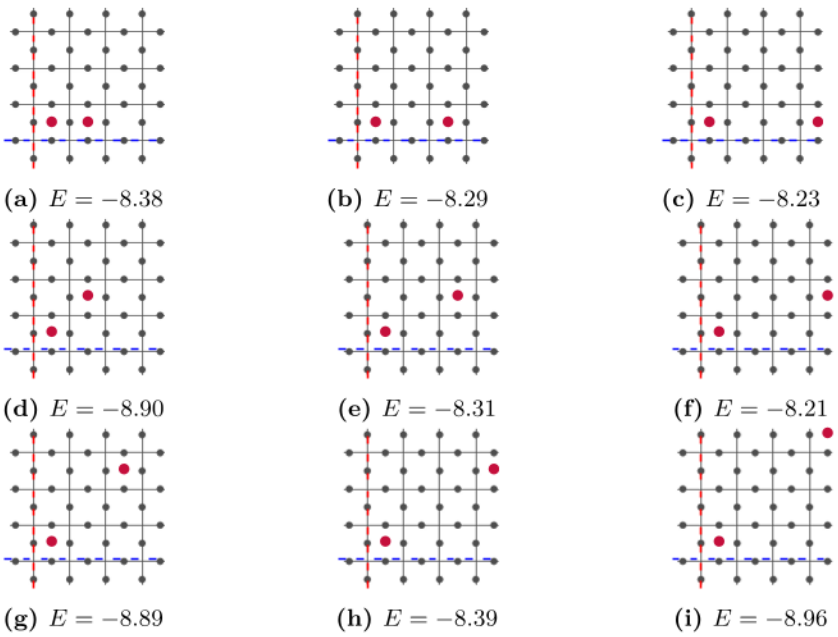

(a) $E = -8.38$ **(b)** $E = -8.29$ **(c)** $E = -8.23$

(d) $E = -8.90$ **(e)** $E = -8.31$ **(f)** $E = -8.21$

(g) $E = -8.89$ **(h)** $E = -8.39$ **(i)** $E = -8.96$

Figure V.2: The red dots give the plaquette with eigenvalue -1 and the energies are the ground state energies calculated with both Wilson loop operators giving the eigenvalue $+1$.

compared to other processes. Especially the comparison to the process shown in subfigure d is interesting, because here the ground state energy in the final state is the same as in the state we start with, but in the process one would create fractons because the excitation is not moved on a diagonal. We conclude that the calculation is consistent with behavior similar to lineons.

V.3 Completely flippable states and four plaquette excitations

We now give arguments that the symmetry sector with four plaquette excitations placed on a rectangle has the lowest ground state energy. For this, we discuss the existence of so called completely flippable states.

We call a product state completely flippable if it is built up by only flippable stars, as seen in Figure IV.3. Also, stars not placed on the checkerboard lattice have to be flippable so that for every star, $\tilde{A}_s |\Psi\rangle \neq 0$. Such states are connected to most other product states in the corresponding symmetry sector. We expect a symmetry sector without such states to have a higher ground state energy than a symmetry sector with completely flippable states due to more quantum fluctuations. We also verified by ED

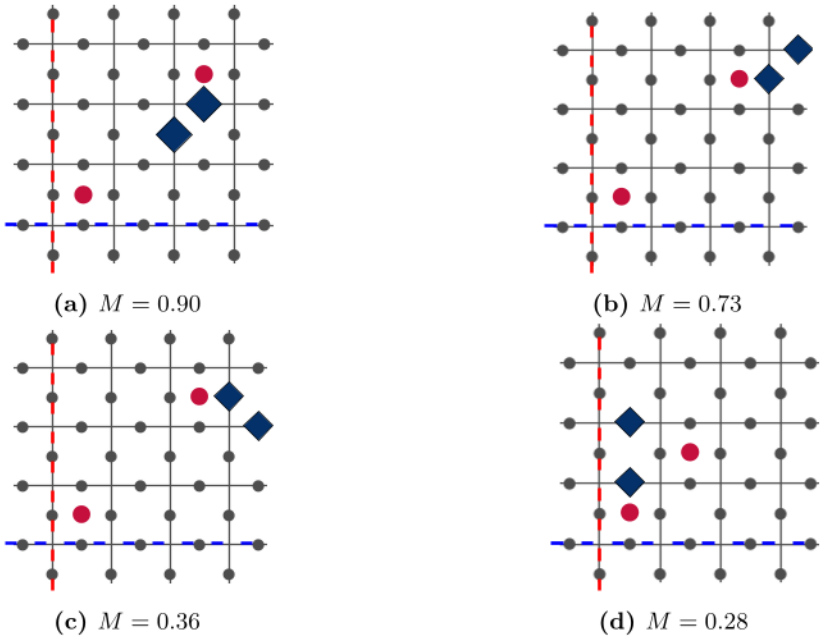

(a) $M = 0.90$ **(b)** $M = 0.73$ **(c)** $M = 0.36$ **(d)** $M = 0.28$

Figure V.3: The overlap of groundstates M calculated for processes where the eigenvalues for the plaquettes on the red dots were chosen to be -1 and the σ^x Matrices act on the blue rhombuses. Again the Wilson loop eigenvalues are set to $+1$.

that the product states with the highest amplitude in the ground state are completely flippable.
The only symmetry sectors with completely flippable states and all B_p eigenvalues equal to $+1$ are the ones that host a global ground state. We can see this with the same argument as seen in Chapter 3. The local ground states on the checkerboard lattice are sums of completely flippable states, so if there is no global ground state in the checkerboard $U(1)$ toric code, we cannot find a state with completely flippable product states. For the checkerboard $U(1)$ toric code, we found that the ground states are in the same symmetry sectors as the ones of the $U(1)$ toric code.
In the next step, we discuss the symmetry sectors where the constraint $B_p |\Phi\rangle = |\Phi\rangle$ is violated four times. In the same fashion as in Chapter 4 we argue, that a plaquette with an eigenvalue of -1 restricts one of the stars on the anti-diagonal to be in the state $|1\rangle$ or $|\bar{1}\rangle$ and one on the diagonal has to be in the state $|-1\rangle$ $|-\bar{1}\rangle$ as seen in Figure V.4. If we require that all stars are flippable, a plaquette now constrains two diagonals. On the checkerboard, one would be a diagonal on the white squares and the other on the black squares. We choose periodic boundary conditions. So the diagonal winds around the torus and would meet the star constraint to be $|0\rangle$ or $|\bar{0}\rangle$. To fulfill the requirement that all stars are flippable, we have to choose two more plaquettes on

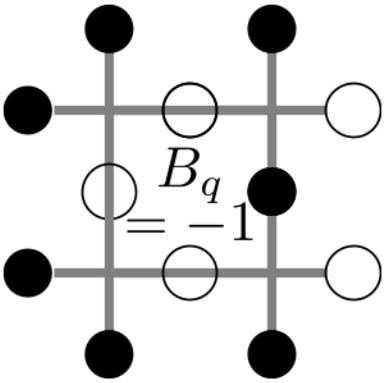

Figure V.4: If one does not restrict only the stars one a checkerboard to be flippable, two product states sharing two spins with the plaquette are restricted.

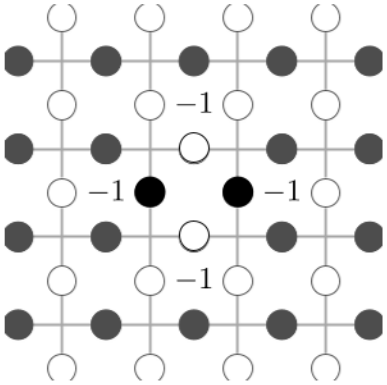

Figure V.5: A completely flippable state with four plaquette excitations placed on a rectangle.

the diagonal and anti-diagonal to fulfill the condition that $B_p |\Phi\rangle = -|\Phi\rangle$. These two restrict one more diagonal to be in the states $|+1\rangle$ or $|-1\rangle$. At the plaquette where both of the diagonals meet, we need another plaquette to give the eigenvalue -1. A example of such a state can be seen in Figure V.5.

They could either meet at the last corner of a rectangle or at a second plaquette where the diagonal meet. But if they meet at the second plaquette not on the rectangle the requirement that all stars are flippable can still not be fulfilled as verified with ED.

This way, we see that four plaquettes excitations on a rectangle are needed for a completely flippable state in a symmetry sector where the constraint $B_p |\Psi\rangle = |\Psi\rangle$ is violated.

V.4 Four particle states with ED

With the argument before, we expect symmetry sectors where all plaquette excitations sit on a square to have the lowest energy. In Figure V.6 we find, that this indeed holds true, although some symmetry sectors like the one labeled d, are rather close in energy.

But placing the plaquette excitations in a way fractons would be necessary in the lowest energy state even for lineons is energetically unfavorable like seen in Figure V.6.

It is not clear from system sizes this small if the plaquette excitations can be considered as fractons, since placing them on a square is most favorable, or lineons. In Figure V.7

the overlap between ground states and moved states was calculated for some processes. We find that the process that moves the plaquette excitations on a rectangle has the largest overlap with the ground state in the other symmetry sector. This would be consistent with fractonic excitations, since by moving only one particle away from the rectangle we have to create an excitation.

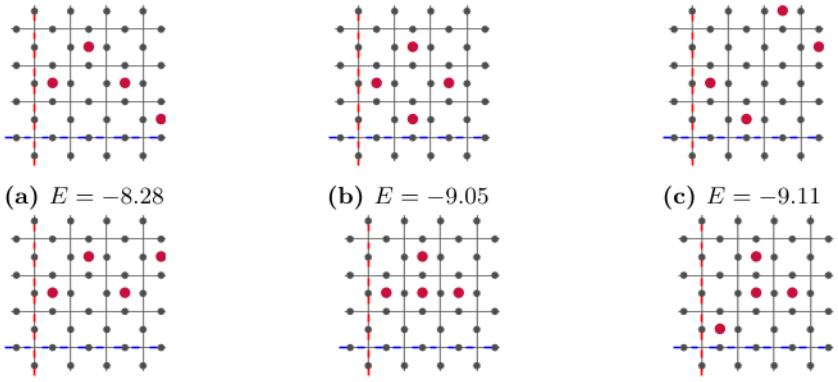

(a) $E = -8.28$ **(b)** $E = -9.05$ **(c)** $E = -9.11$

(d) $E = -8,89$ **(e)** $E = -8,24$ **(f)** $E = -8,82$

Figure V.6: The red dots indicate the plaquette with eigenvalue -1 and the energies are the ground state energies calculated with both Wilson loop operators giving the eigenvalue $+1$.

V.5 Discussion

In this section, the results of the previous sections are discussed. For a finite system, we looked for signatures of fractonic excitations in the ground state energy of different symmetry sectors. We found that plaquette excitations placed on a diagonal have a ground state lower in energy, which would fit the description of those as lineons. We also gave a heuristic argument that four plaquette excitations may behave like fractons and not like lineons because of the absence of completely flippable states and verified this claim for small systems although finite size effects make it hard to draw a conclusion. Regarding confinement, no conclusions can be drawn. We can now put the heuristic argument given in Ref. [9] in the context of fracton excitations. Assuming the phase of the $U(1)$-toric code hosts lineons as plaquette excitations, we could move them on a diagonal around the torus to change the eigenvalues of both Wilson loop operators without facing an energy barrier. This process would correspond to the T^{45° operator discussed in Chapter 3. The three fold ground state degeneracy can still not be explained easily this way.

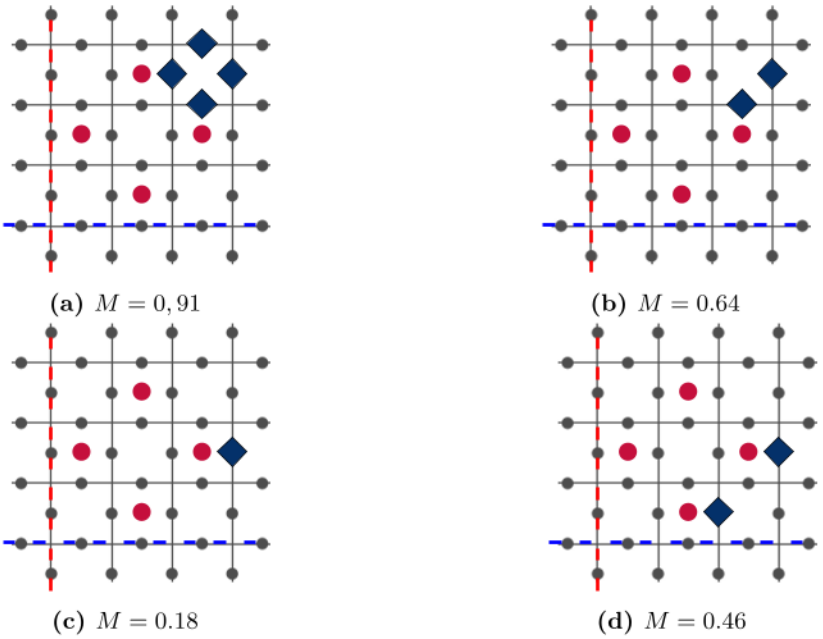

(a) $M = 0,91$ **(b)** $M = 0.64$

(c) $M = 0.18$ **(d)** $M = 0.46$

Figure V.7: The overlap M calculated for processes with 4 plaquette excitations.

VI Summary and outlook

In this thesis, the $U(1)$ toric code was studied [9]. For this, the checkerboard $U(1)$ toric code was introduced. This Hamiltonian reproduces the $U(1)$ toric code in one limit and is exactly solvable in another one. The exactly solvable limit was discussed, and a subextensive ground state degeneracy was found. The ground states in this limit lie in the same symmetry sectors for different compactifications, like the ground states found in the $U(1)$ toric code in Ref. [9]. By using degenerate perturbation theory, we found that the different ground states only couple in order L but the ground state degeneracy is still lifted in order four. Further, the gap between the states in the ground state manifold for $\lambda_{A''} = 0$ and the global ground state grows subextensively. The excitations with a gap of $O(1)$ in system size were discussed, and a non-topological fracton phase was found. One of the excitation types behaves as a lineon, and the other type of excitation as type 1 fractons. The subextensive gap, which is infinite in the thermodynamic limit, is small for all finite systems. Indeed, for $L = 16$ it is so small, that if the series expansion is still valid for $\lambda_{A''} = 1$ it would lie within the error bars of the QMC simulation of Ref. [9] and would not be detected. This opens the possibility that the phase found in the checkerboard $U(1)$ toric code is adiabatically connected to the one of the $U(1)$ toric code. This would be in contradiction to the suggestion in Ref. [9] for topological order. The other possibility would be a quantum phase transition to another phase. The obvious and most important continuation of this work is to look for a phase transition between the topologically ordered phase and the non-topologically confined phase. One could look for a phase transition using high order series expansion like done in Ref. [39, 12, 45] or QMC like in Ref. [12, 38]. One could also try to improve on the QMC results of Ref. [9] to narrow the potential size of the gap between the different topological sectors further down. Even if there is no phase transition, the system remains interesting because of the fractonic excitations and the potential experimental implementation mentioned in Ref. [9]. So one could look for phase transitions if a magnetic field is applied to the chckerboard $U(1)$ toric code like it was done for the usual toric code in Ref. [45]. If between $\lambda_{A''} = 0$ and $\lambda_{A''} = 1$ a phase transition indeed occurs, a further investigation of the phase of the $U(1)$ toric code would be needed. In this work, heuristic arguments and numerical results for small systems were given that suggest that the plaquette excitations in this phase are still fractons. This would be interesting because two-dimension, topological

ordered fracton phases were believed to be impossible [43]. But recently a non trivial example for such a phase was found in Ref. [44].

Another extension of the work could be to study the relationship between dynamic constraints and fractonic excitations further. Enriching the $U(1)$ toric code with the global $U(1)$ symmetry imposes dynamic constraints on the loop dynamics [9]. We found that imposing these dynamic constraints may lead to fractonic excitations. So the question arises if there is a more general connection between imposing dynamic constraints on a system and the peculiar properties of the $U(1)$ toric code.

Bibliography

[1] Swendsen Robert H. An introduction to statistical mechanics and thermodynamics. Oxford Uni. Press, New York, 2012.

[2] David Tong. Lectures on the quantum hall effect. 2016.

[3] Xiao-Gang Wen. Topological order: From long-range entangled quantum matter to a unified origin of light and electrons. ISRN Condensed Matter Physics, 2013:1–20, March 2013.

[4] Jiannis K. Pachos. Introduction, page 3–12. Cambridge University Press, 2012.

[5] A.Yu. Kitaev. Fault-tolerant quantum computation by anyons. Annals of Physics, 303(1):2–30, January 2003.

[6] K. J. Satzinger et. al. Realizing topologically ordered states on a quantum processor. Science, 374(6572):1237–1241, 2021.

[7] Claudio Chamon, Dmitry Green, and Zhi-Cheng Yang. Constructing quantum spin liquids using combinatorial gauge symmetry. Physical Review Letters, 125(6), August 2020.

[8] Claudio Chamon, Dmitry Green, and Andrew J. Kerman. Superconducting circuit realization of combinatorial gauge symmetry. PRX Quantum, 2:030341, Sep 2021.

[9] Kai-Hsin Wu, Alexey Khudorozhkov, Guilherme Delfino, Dmitry Green, and Claudio Chamon. $u(1)$ symmetry enriched toric code. Phys. Rev. B, 108:115159, Sep 2023.

[10] Michael Pretko, Xie Chen, and Yizhi You. Fracton phases of matter. International Journal of Modern Physics A, 35(06):2030003, February 2020.

[11] Rahul M. Nandkishore and Michael Hermele. Fractons. Annual Review of Condensed Matter Physics, 10(1):295–313, March 2019.

[12] V. Kott, M. Mühlhauser, J. A. Koziol, and K. P. Schmidt. Quantum robustness of the toric code in a parallel field on the honeycomb and triangular lattice, 2024.

[13] Kai Phillip Schmidt. Persisting topological order via geometric frustration. Phys. Rev. B, 88:035118, Jul 2013.

[14] M. F. Araujo de Resende. A pedagogical overview on 2d and 3d toric codes and the origin of their topological orders. Reviews in Mathematical Physics, 32(02):2030002, August 2019.

[15] David A. Reiss and Kai P. Schmidt. Quantum robustness and phase transitions of the 3d toric code in a field. SciPost Physics, 6(6), June 2019.

[16] Pablo Sala, Tibor Rakovszky, Ruben Verresen, Michael Knap, and Frank Pollmann. Ergodicity breaking arising from hilbert space fragmentation in dipole-conserving hamiltonians. Phys. Rev. X, 10:011047, Feb 2020.

[17] Vedika Khemani, Michael Hermele, and Rahul Nandkishore. Localization from hilbert space shattering: From theory to physical realizations. Phys. Rev. B, 101:174204, May 2020.

[18] Joshua M Deutsch. Eigenstate thermalization hypothesis. Reports on Progress in Physics, 81(8):082001, July 2018.

[19] Sanjay Moudgalya, B Andrei Bernevig, and Nicolas Regnault. Quantum many-body scars and hilbert space fragmentation: a review of exact results. Reports on Progress in Physics, 85(8):086501, July 2022.

[20] Oliver Hart and Rahul Nandkishore. Hilbert space shattering and dynamical freezing in the quantum ising model. Physical Review B, 106(21), December 2022.

[21] Federico Balducci, Andrea Gambassi, Alessio Lerose, Antonello Scardicchio, and Carlo Vanoni. Localization and melting of interfaces in the two-dimensional quantum ising model. Physical Review Letters, 129(12), September 2022.

[22] Federico Balducci, Andrea Gambassi, Alessio Lerose, Antonello Scardicchio, and Carlo Vanoni. Interface dynamics in the two-dimensional quantum ising model. Physical Review B, 107(2), January 2023.

[23] Roderich Moessner and Joel E. Moore. Topological Phases of Matter. Cambridge University Press, 2021.

[24] Nathan Seiberg and Shu-Heng Shao. Exotic symmetries, duality, and fractons in 2+1-dimensional quantum field theory. SciPost Phys., 10:027, 2021.

[25] Nathan Seiberg and Shu-Heng Shao. Exotic $U(1)$ symmetries, duality, and fractons in 3+1-dimensional quantum field theory. SciPost Phys., 9:046, 2020.

[26] Diego Delmastro and Jaume Gomis. Symmetries of abelian chern-simons theories and arithmetic, 2021.

[27] Masaki Oshikawa, Yong Baek Kim, Kirill Shtengel, Chetan Nayak, and Sumanta Tewari. Topological degeneracy of non-abelian states for dummies. Annals of Physics, 322(6):1477–1498, 2007.

[28] M Takahashi. Half-filled hubbard model at low temperature. Journal of Physics C: Solid State Physics, 10(8):1289, apr 1977.

[29] Claudio Chamon. Quantum glassiness in strongly correlated clean systems: An example of topological overprotection. Phys. Rev. Lett., 94:040402, Jan 2005.

[30] Jeongwan Haah. Local stabilizer codes in three dimensions without string logical operators. Physical Review A, 83(4), April 2011.

[31] Sagar Vijay, Jeongwan Haah, and Liang Fu. Fracton topological order, generalized lattice gauge theory, and duality. Physical Review B, 94(23), December 2016.

[32] Michael Pretko. Subdimensional particle structure of higher rank $u(1)$ spin liquids. Phys. Rev. B, 95:115139, Mar 2017.

[33] Andrey Gromov, Andrew Lucas, and Rahul M. Nandkishore. Fracton hydrodynamics. Physical Review Research, 2(3), July 2020.

[34] Abhinav Prem, Jeongwan Haah, and Rahul Nandkishore. Glassy quantum dynamics in translation invariant fracton models. Physical Review B, 95(15), April 2017.

[35] Michael Pretko and Leo Radzihovsky. Fracton-elasticity duality. Phys. Rev. Lett., 120:195301, May 2018.

[36] Michael Pretko. Emergent gravity of fractons: Mach's principle revisited. Phys. Rev. D, 96:024051, Jul 2017.

[37] Yizhi You, Julian Bibo, Frank Pollmann, and Taylor L. Hughes. Fracton critical point at a higher-order topological phase transition. Phys. Rev. B, 106:235130, Dec 2022.

[38] Zheng Zhou, Xue-Feng Zhang, Frank Pollmann, and Yizhi You. Fractal quantum phase transitions: Critical phenomena beyond renormalization. 2021.

[39] Raymond Wiedmann, Lea Lenke, Matthias Mühlhauser, and Kai Phillip Schmidt. Absence of fractal quantum criticality in the quantum newman-moore model. Phys. Rev. Res., 6:013191, Feb 2024.

[40] Daniel Adler, David Wei, Melissa Will, Kritsana Srakaew, Suchita Agrawal, Pascal Weckesser, Roderich Moessner, Frank Pollmann, Immanuel Bloch, and Johannes Zeiher. Observation of hilbert-space fragmentation and fractonic excitations in two-dimensional hubbard systems. 2024.

[41] Kenneth G. Wilson. Confinement of quarks. Phys. Rev. D, 10:2445–2459, Oct 1974.

[42] Lucile Savary and Leon Balents. Quantum spin liquids: a review. Reports on Progress in Physics, 80(1):016502, November 2016.

[43] David Aasen, Daniel Bulmash, Abhinav Prem, Kevin Slagle, and Dominic J. Williamson. Topological defect networks for fractons of all types. Phys. Rev. Res., 2:043165, Oct 2020.

[44] Guilherme Delfino, Claudio Chamon, and Yizhi You. 2d fractons from gauging exponential symmetries. 2023.

[45] Sébastien Dusuel, Michael Kamfor, Román Orús, Kai Phillip Schmidt, and Julien Vidal. Robustness of a perturbed topological phase. Physical Review Letters, 106(10), March 2011.

Eigenständigkeitserklärung

Ich versichere, dass ich diese Arbeit selbstständig verfasst habe. Alle Stellen, die sinngemäß oder wörtlich aus anderen Quellen entnommen sind, sind als solche gekennzeichnet. Ich habe keine anderen als die angegebenen Quellen und Hilfsmittel benutzt. Die Arbeit wurde keiner anderen Stelle zur Prüfung vorgelegt.

Ort, Datum

Maximilian Vieweg

Danksagung

Bedanken möchte ich mich an erster Stelle bei Kai, der ein sehr spannendes Thema für diese Arbeit vorgeschlagen hat, und auch trotz eines vollen Terminkalender immer Zeit für Treffen gefunden hat, um diese Arbeit perfekt zu betreuen. Bei Andi, Viktor und Lea möchte ich mich für die vielen hilfreichen Diskussionen in den Meetings und auch außerhalb bedanken. Insgesamt möchte ich mich beim gesamten Lehrstuhl für die schöne Zeit und die langen Kaffeepausen bedanken. Auch bei meiner Familie möchte ich mich für die Unterstützung während meines Studiums bedanken.